CT-755 SSI – 2013
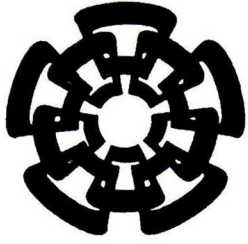
Don – 2014

Centro de Investigación y de Estudios Avanzados
del Instituto Politécnico Nacional
Unidad Guadalajara

Control Óptimo Inverso Híbrido Inteligente para un Proceso de Digestión Anaeróbica

Tesis que presenta:
Kelly Joel Gurubel Tun

Para obtener el grado de:
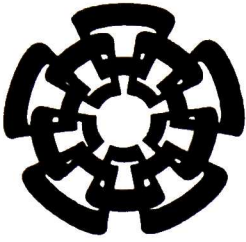**Doctor en Ciencias**

en la especialidad de:
Ingeniería Eléctrica

Directores de Tesis
Dr. Edgar Nelson Sánchez Camperos
Dr. Salvador Carlos Hernández

CINVESTAV del IPN Unidad Guadalajara, Guadalajara, Jalisco, Junio de 2013.

Centro de Investigación y de Estudios Avanzados
del Instituto Politécnico Nacional
Unidad Guadalajara

Hybrid Intelligent Inverse Optimal Control for an Anaerobic Digestion Process

A dissertation presented by·
Kelly Joel Gurubel Tun

to obtain the degree of:
Doctor in Science

in the subject of:
Electrical Engineering

Thesis Advisors
Dr. Edgar Nelson Sánchez Camperos
Dr. Salvador Carlos Hernández

Control Óptimo Inverso Híbrido Inteligente para un Proceso de Digestión Anaeróbica

Tesis de Doctorado en Ciencias
Ingeniería Eléctrica

Por:

Kelly Joel Gurubel Tun

Maestro en Ciencias en Ingeniería Eléctrica
Centro de Investigación y Estudios Avanzados del IPN
Unidad Guadalajara 2007-2009

Directores de Tesis
Dr. Edgar Nelson Sánchez Camperos
Dr. Salvador Carlos Hernández

CINVESTAV del IPN Unidad Guadalajara, Junio de 2013.

Resumen

Motivado por el rápido crecimiento de la demanda de electricidad, el agotamiento de los combustibles fósiles y la conciencia ambiental, los países desarrollados empezaron a investigar la posibilidad de utilizar eficientemente las fuentes de energía renovables. En los últimos años, con distintos grados de éxito, diferentes fuentes de energía renovables han sido estudiadas para la generación de energía eléctrica; entre ellos, geotérmica, biomasa, solar, eólica, hidroeléctrica por microturbinas y por las mareas. La biomasa es atractiva como un recurso potencial de energía debido a que las fuentes de petróleo no son ilimitadas, mientras que la biomasa es renovable. La sustitución de combustibles fósiles con biomasa reduciría las emisiones de dióxido de carbono neto a la atmosfera. Además, los combustibles de biomasa tienen un calor de combustión razonable así como bajo contenido en azufre, ceniza y nitrógeno en comparación con muchos carbones y aceites. Los derivados de la biomasa tal como hidrógeno, etanol, metanol y metano pueden ser convertidos en formas de energía como calor, vapor y electricidad. La digestión anaeróbica es un proceso biológico en el que la materia orgánica (sustrato) se degrada por microorganismos (biomasa), en ausencia de oxígeno, produciendo biogás (metano y dióxido de carbono) y residuos orgánicos estables. Los procesos anaeróbicos son muy atractivos debido a sus propiedades de tratamiento de residuos y su capacidad para la producción de metano, que puede ser utilizado para la generación de energía eléctrica. El proceso se desarrolla en cuatro etapas sucesivas: hidrólisis, acidogénesis, acetogénesis y metanogénesis. La metanogénesis es la etapa lenta; ésta impone las dinámicas del proceso y es considerada como la etapa limitante. En estos procesos anaeróbicos existen variables difíciles de medir o que no se pueden medir, que son necesarias para el control de procesos. Los observadores y sensores son una alternativa viable para la estimación de este tipo de variables. Un enfoque interesante para evitar el problema asociado a los observadores de estado basados en el modelo, es el observador neuronal. En esta tesis, se propone el uso de un observador neuronal no lineal en tiempo discreto ("Recurrent High Order Neural Observer", RHONO) para sistemas no lineales desconocidos en presencia de perturbaciones externas e incertidumbre de parámetros. Este observador es empleado para estimar la concentración de biomasa, degradación del sustrato y carbono inorgánico en un proceso de digestión anaeróbica de tratamiento de aguas residuales. Estas variables son buenos indicadores de la actividad biológica dentro del reactor continuamente agitado ("Continuous Stirred Tank Reactor", CSTR), y son utilizadas para monitorear el proceso. Una validación experimental para el observador usando datos reales de un proceso a escala es incluida en este trabajo. El objetivo es la producción de metano para la generación de energía, por lo tanto la digestión anaeróbica es desarrollada en un CSTR con biomasa inmovilizada en un soporte sólido, y la etapa limitante es modelada considerando estas condiciones. La producción de metano se obtiene por forzar al sistema dinámico de digestión anaeróbica a seguir una trayectoria de referencia de dicho gas. Para alcanzar esto, se utiliza una estrategia de control óptimo inverso inteligente híbrido con gradiente de velocidad para seguimiento de trayectorias. La ley de control calcula la tasa de dilución y la adición de bicarbonato necesarios para forzar al sistema a seguir la trayectoria y evitar la inhibición del proceso. El controlador propuesto se basa en el modelo del RHONO y control óptimo inverso en tiempo discreto. La aplicabilidad de la estrategia propuesta se ilustra mediante simulaciones.

Abstract

Motivated by the rapid growth of electricity demand, considering the depletion of fossil fuels, and due to increased environmental awareness, developed countries began to investigate the possibility of using renewable energy sources efficiently. In recent years, with varying degrees of success, different renewable energy sources have been and continue to be studied for electric power generation, among them, geothermal, biomass, solar, wind, hydropower by micro-turbines and tidal waves. Biomass is attractive as a potential energy resource, because the amount of oil sources is not unlimited, while biomass is renewable. Replacing fossil fuels with biomass would reduce the net carbon dioxide emissions into the atmosphere. Moreover, biomass fuels have a reasonable heat of combustion, and they usually have low sulfur, nitrogen and ash content as compared to many coals and oils. Derived from biomass such as hydrogen, ethanol, methanol, and methane may be converted to energy forms as heat (via burning), steam and electricity. Anaerobic digestion is a biological process in which organic matter (substrate) is degraded by micro-organisms (biomass), in absence of oxygen. Such degradation produces biogas (methane and carbon dioxide), and stable organic residues. Anaerobic processes are very attractive because of their waste treatment properties and their capacity for generating methane from waste materials, which can be used for electrical energy generation. The process is developed in four successive stages: hydrolysis, acidogenesis, acetogenesis and methanogenesis. Methanogenesis, is considered the limiting stage because is the slowest one and imposes the dynamics of the process. In these anaerobic processes there exist hardly measurable or unmeasurable variables which are necessary for process control. Observers and soft sensors are an interesting alternative in order to estimate these kinds of variables. An interesting approach for avoiding the associated problem of model-based state observers is the neural network observer. Neural observer based on a discrete-time recurrent high-order neural network (RHONN) trained with an extended Kalman filter (EKF) based algorithm has proven to be effective for biological processes. In this work, a nonlinear discrete-time neural observer (RHONO) for unknown nonlinear systems in presence of external disturbances and parameter uncertainties is used to estimate the biomass concentration, substrate concentration and inorganic carbon in an anaerobic process digestion for wastewater treatment. These variables are good indicators of the biological activity inside the reactor; they are used for monitoring the process. An experimental validation for the observer using real data from a lab scale process is included in this dissertation. The objective is methane production for energy generation, therefore anaerobic process is developed in a continuously stirred tank reactor (CSTR), with immobilized biomass on a solid support, and limiting stage is modeled considering this conditions. Methane production is obtained by forcing the dynamic system from anaerobic digestion to track a trajectory reference of mentioned gas. In order to reach this, a hybrid intelligent speed-gradient inverse optimal control for trajectory tracking is applied. The control law calculates dilution rate and bicarbonate addition in order to force the system to track a trajectory and avoiding the inhibition process. The proposed controller is based on discrete-time RHONN model and discrete-time inverse optimal control. The applicability of the proposed scheme is illustrated via simulations.

Acknowledgments

Notations and Acronyms

Notations

$\forall$	for all
$\in$	belonging to
$\Rightarrow$	implies
$\subset$	contained in
$\subseteq$	contained in or equal to
$\cup$	union
$\cap$	intersection
$:=$	equal by definition
$\lambda_{max}(Q)$	the minimum eigenvalue of matrix Q
$\lambda_{min}(Q)$	the maximum eigenvalue of matrix Q
$P > 0$	a positive definite matrix P
$P \geq 0$	a positive semidefinite matrix P
ΔV	denotes the Lyapunov diference
$\leq$	less than or equal to
A	set or vector space
$\mathcal{K}$	denotes a class $\mathcal{K}$ function
$\mathcal{K}_\infty$	denotes a class $\mathcal{K}_\infty$ function
$\mathcal{KL}$	denotes a class $\mathcal{KL}$ function
N	the set of all natural numbers
Z^+	the set of nonnegative integers
R	the set of all real numbers
R^+	the set of positive real numbers
R^n	n-dimension vector space
$(\cdot)^T$	denotes transpose
$(\cdot)^{-1}$	denotes inverse
$(\cdot)^*$	denotes optimal function
$\|x\|_n$	the n-norm of vector x
$\|x\|$	the Euclidean norm of vector x

Acronyms

AD	Anaerobic Digestion
COD	Chemical Oxygen Demand
CLF	Control Lyapunov Function
DT	Discrete-Time
EKF	Extended Kalman Filter
GS	Globally Stable
GAS	Globally Asymptotically Stable
HJB	Hamilton-Jacobi-Bellman
LTI	Linear Time Invariant
MI	Matrix Inequality
PID	Proportional Integral Derivative
PSO	Particle Swarm Optimization
RHONO	Recurrent High Order Neural Observer
RHONN	Recurrent High Order Neural Network
RNN	Recurrent Neural Networks
RCLF	Robust Control Lyapunov Function
SG	Speed-Gradient
TS	Takagi-Sugeno
VFA	Volatile Fatty Acids

Contents

Chapter 1

Introduction

1.1 State of the art

The rapid increase of wastewater due to domestic, industrial and agricultural activities requires careful consideration by all society sectors. Wastewater treatment is necessary to reduce organic and suspended solids loads in order to limit pollution of the environment. One of the more adequate methods for wastewater treatment is anaerobic digestion. It provides a wide variety of advantages including environmental benefits, as well as economic ones. Anaerobic processes are very attractive because of their waste treatment properties and their capacity for generating methane from waste materials, which can be used for electrical energy generation [1], [2], [3]. However, anaerobic digestion is a **sensible process** to operating conditions variations, such as pH, temperature, hydraulic and organic overloads, among others.

In biological processes, there exist hardly measurable or unmeasurable variables which are necessary for process supervision and control [4]. Then, estimation and control strategies are required in order to guarantee adequate performance. Nowadays, there exist commercial biogas sensors, which allow methane and carbon dioxide to be measured on-line [5], [6]. However, substrate and biomass measures are more restrictive. The existing biomass sensors are quite expensive, are designed from biological viewpoint (based on capacitance or turbidity properties), and they are not reliable for control purposes. Furthermore, substrate measure is done off-line by chemical analysis, which requires at least two hours; then, state observers are an interesting alternative in order to deal with this situation. Hence, observer design is a major problem to be solved, in addition to adequate sensors selection. Along this line, the essential idea is to develop virtual sensors with the purpose of considering variables of difficult access, which are of crucial importance for control applications. In the literature, different observers have been proposed. Adaptive observer [7], for nonlinear cascade state affine systems gives a reliable tool towards the control design considering integrative information about no physically measured states and sensitive parameters of the model. Based in sensitivity analysis, the proposed nonlinear adaptive observer is able to estimate the most sensitive parameters and system states with an arbitrarily tunable rate. This observer is tested for acidogenic and methanogenic bacteria concentration estimations, as well as growth rate parameter estimations for an AD process. Convergence of estimated states and parametric estimation is verified. For this methodology is important to remark that, in order to obtain an adaptive observer for n states, first step

must be to describe the system as a n cascade affine subsystems which states and outputs are defined for each one. In [8], [9] a reset adaptive observer (ReAO) for nonlinear systems is presented. ReAO is an adaptive observer consisting of an integrator and a reset law that resets the output of the integrator depending on a predefined reset condition. The inclusion of reset elements can improve the observer performance but it can also destroy the stability of the estimation process if the ReAO is not properly tuned. The observer gains as well as the reset element parameters are optimally chosen by solving the L_2 gain minimization problem, which can be rewritten as an equivalent LMI problem. The two most popular reset conditions within the reset time independent framework are zero crossing and sector condition. The main advantage of ReAOs is that potentially much richer feedback signals can be obtained by resetting some observer states. Since the method is based on minimizing the L_2 gain of the ReAO, the stability and convergence of the estimation process are guaranteed. An exception would be when the system is affected by disturbances with a steady-state offset, since the ReAO might need more time to reject the effect of the disturbance on the unknown variables. Interval observer [10], [11] is a good alternative to diminish the effects of the system uncertainties; nevertheless, the convergence rate of the estimation cannot be tune. Furthermore, an over-estimation effect in the considered intervals can be induced. Finally, a nonlinear discrete-time neural observer (RHONO) for unknown nonlinear systems in presence of external disturbances and parameter uncertainties is proposed in [12], [13]. This neuronal observer based in recurrent high order neural network (RHONN) has proven to be effective for biological processes. An artificial neural network (NN) consists of a finite number of neurons (structural element), which are interconnected to each other; they are inspired from biological neural networks. Recurrent neural networks have at least one feedback loop, which improves the learning capability and performance of the network [14]. This structure also offers a better suited tool to model and control nonlinear systems [15]. RHONN are a generalization of the first-order Hopfield networks [16]. The main advantages that offer this neural network are their high performance and its low level of complexity and tuning; additionally, the knowledge of the model is not strictly necessary.

Simultaneously, **an increasing interest has been developed to improve the operation of the bio-processes** through the application of advanced schemes of control [17], [18]. The control objectives focus in the regulation of the pollution, biogas production and maintaining the stability of the process; this is done in order to reduce the production costs, to increase the biogas production and to conserve quality of the byproducts. With the purpose of facing the challenges that anaerobic digestion imposes, as sensitivity to changes in the operating conditions, the uncertainties in the parameters of the process and the highly nonlinear dynamics, several techniques of control have been implemented. Fuzzy PID control for nonlinear AD process is proposed in [19], [20]. For control of the PH in the system, an automatic dosing system is installed and strong acid (hydrochloric acid) and strong base (sodium hydroxide) are adopted as neutralizing liquid in the process. pH is required to be controlled within 6.8 to 7.2. Fuzzy PID control determines the controlled variable according to control rules and on-line detection results instead of a precise mathematical model. Furthermore, fuzzy PID control can well solve the difficult problems in an anaerobic biological treatment system such as difficult precise model building, large lagging, strong disturbance and multiple variables. The pH control of the anaerobic wastewater treatment system is an indispensable measurement item; however, it is difficult to control, for there are numerous phenomena that cannot be described quantitatively. There is pure lagging at the mixing, measuring and other links in the PH control process, so that the regulated amount fails to reflect the perturbation borne by the system in

time. The robust control [21], [22] allows a suitable process operation independent of dynamic changes; although, it presents the disadvantage that is necessary to predefine uncertainties limits. Adaptive control strategies were developed to take into account the nonlinearities and the nonstationary features of the digestion process [23]. Such strategies **depart from a physical (mass balance) model of the anaerobic process** to implement simple efficient controllers featuring estimation of physically-related parameters. In fact, model-based controllers have proven to be efficient to regulate nonlinear processes with unknown and unexpected disturbances. Implementation tests of model-based adaptive controllers in pilot-scale [24] and real life scale [25] anaerobic process have been successfully carried out, including extreme input or environmental conditions. Nevertheless, a drawback of adaptive techniques is that linear parametrization is required in order to implement a parameter estimator. In the case of anaerobic processes, it implies that, the inputs are known and bounded, therefore the states and the parameters are bounded [26]. The convergence is not guaranteed when the control input becomes saturated. In [27], neural-fuzzy control system for anaerobic hybrid reactor (AHR) in wastewater treatment and biogas production is proposed. The neural network is used to predict pH, alkalinity and total volatile acids (TVA) variables and then, the fuzzy logic control system use this predicted value as input variables to calculate the daily influent feed flow rate of the AHR that is applied to control and monitor the process response at different operations in the initial, overload influent feeding and the recovery phases. In all three phases, this neural-fuzzy control system show high stability, performance and quick response. However, according to the 4 variables as pH, Alk, TVA and influent feed flow rate associated with 5 terms of membership function (very low, low, medium, high and very high), 625 rules were described and 125 rules were chosen for this fuzzy controller. This mean that for all rules there exist an influent feed flow rate and do not allows the system to operate in open loop, which represents energy saving. On the other hand, Predictive control for AD process is presented in [28], [29]. These model based predictive controllers (MPC) take into account not only the past information, but also predictions of the future behavior of the system, optimizing thus the control effort over an interval of future control inputs. The general control objective is to manipulate the inputs within the operation limits such that a maximum methane production is ensured at all times. Their feed flow rates constitute two model inputs, which are considered as manipulated variables, while the biogas production rate and its methane content constitute two model outputs (controlled variables). The MPC strategy is able to maintain the methane production at a stable output production rate. As disadvantages, the MPC requires define operating range and constraints in the inputs-outputs of the process which guarantee stability. A suitable cost function must be designed such that maximum production is ensured while satisfying stability constraints (i.e. avoid overload). Additionally, it requires a high computational cost. Finally, in [30], [31] speed-gradient inverse optimal neural control is proposed. In this approach, a stabilizing feedback control is designed first such that asymptotic convergence to state reference trajectory is guaranteed, and then it is established that this control optimize a cost functional. The proposed controller is based on a discrete-time (DT) RHONN model and on DT inverse optimal control. Inverse optimal neural control has been applied successfully in mechanical and biological systems. In [30] the applicability of that scheme by trajectory tracking for a two degree of free (DOF) planar robot is illustrated. An on-line series–parallel neural network identifier trained with extended Kalman filter (EKF) is implemented to identify the system with unknown parameters for control synthesis. The goal is to force the angle position to track a desired reference. The goal is achieved because the designed controller maintains stability on the reference for the plant with unknown parameters. In [32]

discrete time inverse optimal trajectory tracking for a class of non-linear positive systems is proposed. The scheme is developed for SISO (simple-input, simple-output) affine systems. This approach is adapted for glycemic control of type 1 diabetes mellitus (T1DM) patients. The control law calculates the insulin delivery rate in order to prevent hyperglycemia levels. A neural model is obtained from an on-line neural identifier, which uses a recurrent neural network, trained with the EKF; simulation results show how the control law is able to stabilize the blood glucose levels along a desired trajectory. Indeed, this scheme improves the regulation of the blood glucose level in T1DM patients, increasing slightly the insulin quantity. This technique is an important result since most of the biological systems are positive ones. Speed-gradient inverse optimal neural control is an adequate and novel algorithm easy to implement.

1.2   Problem Definition

Anaerobic process presents four basic stages: hydrolysis, acidogenesis, acetogenesis and methanogenesis; each one has particular objectives and specific dynamics. Hydrolysis, acidogenesis and acetogenesis are fast stages in comparison with methanogenesis, which is the slowest one; it imposes the dynamics of the process and is considered as the limiting stage. In methanogenesis stage methane is synthesized in two ways: first by acid acetic cleavage, which produces methane and carbon dioxide; and then by CO_2 reduction by hydrogen, which generates CH_4 and water. The acetate reaction is the primary producer of CH_4 because of the limited amount of hydrogen available [33]. Methanogenesis stage is very sensitive to variations on substrate concentration, and biomass increase can be stopped by an excessive substrate production in the previous stages [4]. Depending on the amplitude and duration of these variations, the environment can be acidified avoiding biomass growth and even producing bacteria death; besides, the hydraulic overloads can lead the process to washout (absence of active bacteria inside the reactor). From these situations, substrate concentration and methane production can be blocked and the process is stopped. Then, dilution rate ($D_{in,k}$) and bicarbonate supplying rate ($b_{inc,k}$) are used in order to regulate process pH. $D_{in,k}$ changes reject larger disturbances and supplying $b_{inc,k}$ allows the process to produce a large amount of methane. Monitoring the process behavior and control strategies implementation are important tasks to guarantee an adequate operation. The main idea is to develop efficient unmeasured variables estimation and control actions, easy to implement.

Due to control strategy limitations for anaerobic process, a hybrid intelligent control scheme for an anaerobic wastewater treatment process, which takes place in a CSTR, is proposed. First, a RHONO is designed to estimate hardly measurable or unmeasurable variables which are necessary for monitoring the process and to design hybrid intelligent control. Estimated variables are biomass (X_2), substrate concentration (S_2) and inorganic carbon (IC) in the methanogenesis stage. The observer structure uses the hyperbolic tangent as activation function and is trained using an EKF. This activation function is selected because allows the system dynamic to learn quickly and mathematical calculus are more simples, in comparison with other functions on, [12]. The main advantage of this observer is high performance and reduced complexity. In order to control the AD process, a speed-gradient inverse optimal neural control for trajectory tracking based on the RHONO is considered by its characteristics above mentioned. The controllers determine two control actions, $b_{inc,k}$ and $D_{in,k}$, in order to force the system to track a methane production reference trajectory and avoiding washout. A TS fuzzy supervisor detects the disturbance

amplitude on the input substrate and implements a fuzzy interpolation to obtain the nonlinear reference trajectories. A second TS fuzzy supervisor for scheduling gain is implemented in order to obtain adequate controller gains. Finally, a third TS fuzzy supervisor is implemented in order to apply control actions ($D_{in,k}$ and $b_{inc,k}$) as a function of the operating conditions: if a small input disturbance arrives the supervisor allows the process to operate in open loop, if a large disturbance arrives the supervisor applies the adequate control action ($D_{in,k}$ and $b_{inc,k}$) avoiding washout.

1.3   Objectives

The general objective is to control an AD process, in presence of disturbances, in order to obtain a continue methane production. To do so,, next specific objectives are established:

To synthesize a neural observer in order to estimate variables of the methanogenesis stage and implement a time-varying learning rate in order to improve learning of the neural observer in presence of disturbances.

Perform an experimental validation for the observer in order to verify its performance in presence of disturbances.

To synthesize a control action in order to reject disturbances, to obtain a high efficiency of the process to produce as much biogas as possible and to avoid the process to be stopped.

To synthesize TS fuzzy supervisors, in order to interpolate nonlinear reference trajectories, gains for the controllers and selection among three control actions in presence of different disturbance magnitudes.

To integrate the neural observer, fuzzy supervisors and the control strategy.

To test the hybrid intelligent control scheme in presence of disturbances and parameter variations.

Implement PSO algorithm in order to calculate optimal parameters of the matrices P_C for the control law.

1.4   Dissertation structure

In this dissertation a hybrid intelligent neural control scheme for an anaerobic wastewater treatment processes, which takes place in a CSTR, is proposed.
This dissertation is organized as follows.

In *Chapter 2*, theory preliminaries are introduced, including mathematical model of anaerobic process, neural observer, and an EKF based algorithm training.

Then, *Chapter 3* presents the RHONO structure for state estimation with time-varying learning rate, which is trained on-line using an EKF. This is one of the main contributions of this dissertation, and convergence analysis is stated. The structure is validated via simulations in presence of disturbances and parameter variations. After that, an experimental validation for the observer using real data from a prototype reactor is presented. Later is verified which the structure with time-varying learning rate enhance the NN training and observer is a good alternative to on-line states estimation of the AD process.

Chapter 4 discloses the proposed hybrid intelligent control scheme. Controller design based on the speed-gradient inverse optimal neural control is described. Then, TS fuzzy supervisors for reference trajectories, scheduling gains for the controllers and selection of control actions are presented. Finally, the integrated control strategy is implemented for the AD process and is tested in presence of different disturbances and parameter variations. The convergence analysis of this control scheme is stated. After that, in order to improve the trajectory tracking, PSO optimization algorithm is implemented to calculate the gain matrices of the inverse optimal control law. Later, it is verified that the calculated matrices with the PSO algorithm improve the control law. This overall control strategy is validated via simulations.

Finally, *Chapter 5* presents relevant conclusions and future work.

Chapter 2

Fundamentals

In this chapter, fundamentals of AD processs, required in future chapters are presented. Additionally, a mathematical model of an anaerobic process, a neural observer and an EKF training algorithm, are briefly discussed.

2.1 Anaerobic digestion

Anaerobic digestion is a biological process in which organic matter (substrate) is degraded by anaerobic bacteria (biomass), in absence of oxygen. Such degradation produces biogas (composed primarily of CH_4 and CO_2) and stable organic residues. Anaerobic processes are very attractive because of their waste treatment properties and their capacity for generating methane from waste materials.

2.1.1 Process description

AD process is a complex and sequential process, which consists of four basic stages [17], [34]-[36]:

- Hydrolysis. There, bacteria converts complex organic materials into simpler monomers.
- Acidogenesis. During this stage, soluble monomers are transformed into organic acids, alcohols and volatile fatty acids (VFA) by acidogenic bacteria.
- Acetogenesis. In this third stage, acetogenic bacteria convert VFA into acetic acid, CO_2 and hydrogen.
- Methanogenesis. In this stage methane is produced in two ways; the first one by acid acetic cleavage, which produces CH_4 and CO_2; and the second one by CO_2 reduction with hydrogen, which generates CH_4 and H_2O. The acetate reaction is the primary producer of CH_4 because of the limited amount of hydrogen available [33].

Figure 1 shows the decomposition pathways for major organic and inorganic components of biodegradable wastes.
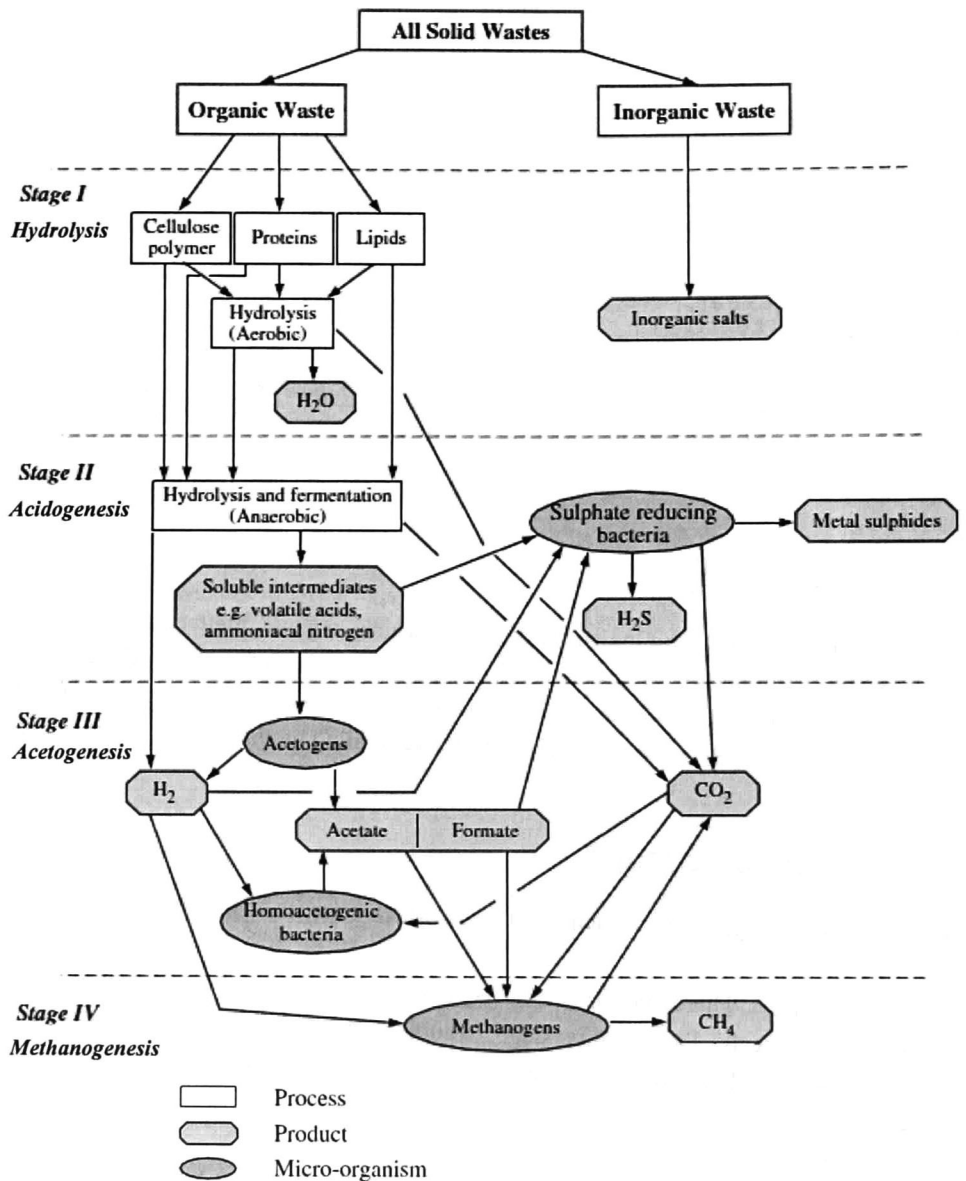
Figure 1 Stages in anaerobic wastewater degradation [36]

Each stage has a specific dynamics. Hydrolysis, acidogenesis and acetogenesis are fast stages in comparison with methanogenesis, which is the slowest one; it imposes the dynamics of the process and is considered as the limiting stage.

2.1.2   Operating conditions

A variety of factors affect the rate of digestion and biogas production. A detailed comparative summary of research on the inhibition of anaerobic processes is presented in [37]. Some of the most important factors are:

- Temperature. Anaerobic bacteria communities can endure temperatures ranging from below freezing to above 57 °C; however they thrive best at about 37 °C (mesophilic conditions).
- pH. The substrate pH is an important parameter for the adequate growth of bacteria and then for wastes transformation. For methanogenesis, the optimal range of substrate pH is between 6.6 and 7. Bicarbonate ions and VFA concentration have an influence on the pH. A pH value higher than 8 causes an inhibition of the bacteria activity, while a value under 5 for a long time produces irreversible damage and death of the bacteria stopping the process due to acidification [4].
- Retention time. For a mesophilic system, ranges from 15 to 30 days are required to waste treatment [33] in order to achieve the complete degradation of the organic materials.

The AD process considered in this dissertation is developed in a scale CSTR (Figure 2) from Cinvestav, Unidad Saltillo with biomass filter, which is used to improve the substrate treatment [38]. Commonly, this operation mode allows a continuous treatment of wastewater, which implies a continuous biogas production.
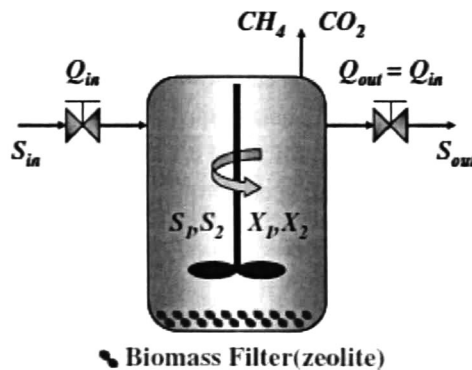
Figure 2 Completely stirred tank reactor with biomass filter.

In practice, the biomass is fixed in a solid support, e.g. zeolite, minerals, synthetic or biologic materials acting as filters. As is shown, the substrate S_{in} is fed to the reactor with a flow rate Q_{in} (L h^{-1}); hence, the dilution rate $D_{in} = Q_{in}/V$ can be determined, where V (L) is the reaction volume. Finally, the treated water goes out at the same flow rate as the input in order to keep a constant volume: $Q_{out} = Q_{in}$.

A illustration of laboratory scale CSTR is shown in Figure 3.
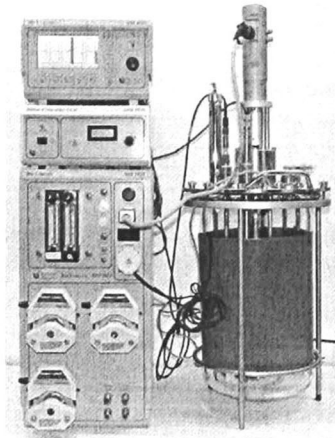
Figure 3 Anaerobic prototype for wastewater treatment

The prototype is an *Applikon®* bioreactor of 7 L, composed by ADI 1010 controller with three control cards: pH, DO_2 (oxygen dissolved) and temperature. ADI 1025 bioconsole, ADI 1032 motor controller, vessel, heating mantle and probes for pH, DO_2 and temperature.

2.1.3   Mathematical model

A functional diagram of AD is proposed in [39], as shown in Figure 4. Biomass is classified as: X_1, corresponding to hydrolytic, acidogenic and acetogenic bacteria and X_2, corresponding to methanogenic bacteria. On the other hand, the organic load is classified in S_1, the components equivalent glucose, which model complex molecules and S_2, the components equivalent acetic acid, which represent the molecules directly transformed in acetic acid. This classification allows the process to be represented by a fast stage, which involves hydrolysis, acidogenesis and acetogenesis and a slow stage, which corresponds mainly to methanogenesis.
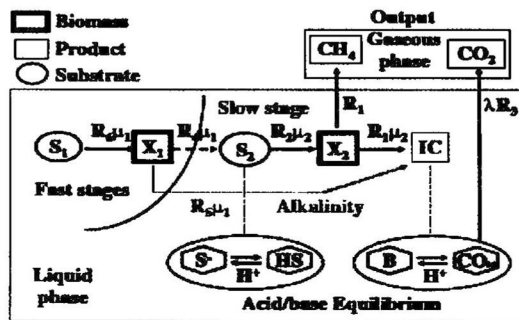
Figure 4 Functional diagram of the anaerobic digestion

Thus, a mathematical model based on both stages is formulated as follows [38], [39]. On one side, the biological phenomena are modeled by ordinary differential equations (1), which represent the dynamical part of the process as:

$$\frac{dX_1}{dt} = \left(\mu_1 - k_{d1}\right)X_1,$$

$$\frac{dS_1}{dt} = -R_6\mu_1 X_1 + D_{in}\left(S_{1in} - S_1\right),$$

$$\frac{dX_2}{dt} = \left(\mu_2 - k_{d2}\right)X_2,$$

$$\frac{dS_2}{dt} = -R_3\mu_2 X_2 + R_4\mu_1 X_1 + D_{in}\left(S_{2in} - S_2\right), \tag{1}$$

$$\frac{dIC}{dt} = R_2 R_3 \mu_2 X_2 + R_5 \mu_1 X_1 - \lambda R_1 R_3 \mu_2 X_2 + D_{in}\left(IC_{in} - IC\right),$$

$$\frac{dZ}{dt} = D_{in}\left(Z_{in} - Z\right)$$

where μ_1 is the growth rate (Haldane type) of X_1 (h^{-1}), μ_2 the growth rate (Haldane type) of X_2 (h^{-1}), k_{d1} the death rate of X_1 (mol L^{-1}), k_{d2} the death rate of X_2 (mol L^{-1}), D_{in} the dilution rate (h^{-1}), S_{1in} the fast degradable substrate input (mol L^{-1}), S_{2in} the slow degradable substrate input (mol L^{-1}), IC inorganic carbon (mol L^{-1}), Z the total of cations (mol L^{-1}), IC_{in} the inorganic carbon input (mol L^{-1}), Z_{in} the input cations (mol L^{-1}), λ is a coefficient considering law of partial pressure for the dissolved CO_2 and $R_1, \ldots, R_6$ are the yield coefficients.

A Haldane type growth rate is selected for this model in order to describe the inhibition by substrate phenomen [40], which allows to include the pH efect and saturation phenomen. The growth rate for X_1 and X_2 are described by equations (2) and (3) respectively:

$$\mu_{1,k} = \frac{\mu_{1max}S_{1,k}}{k_{s1} + S_{1,k} + \dfrac{S_{1,k}HS}{k_{i1}}} \tag{2}$$

$$\mu_{2,k} = \frac{\mu_{2max}HS}{k_{s2} + HS + \dfrac{HS^2}{k_{i2}}} \tag{3}$$

where μ_{1max} (h^{-1}) and μ_{2max} (h^{-1}) are the maximum growth rate for the $X_{1,k}$ and $X_{2,k}$ biomasses respectively, k_{S1} (mol L^{-1}) and k_{S2} (mol L^{-1}) are the growth saturation for the biomasses, k_{i1} (mol L^{-1}) and k_{i2} (mol L^{-1})

are the inhibition constants by substrate excess, HS is non ionized acetic acid (mol L^{-1}) and $S_{l,k}$ (mol L^{-1}) is slow stage substrate.

On the other side, the physical-chemical phenomena (acid-base equilibria and material conservation) are modeled by algebraic equations (4).

$$
\begin{aligned}
&HS + S^- - S_2 = 0, \\
&H^+ S^- - K_a HS = 0, \\
&H^+ B - K_b CO_{2d} = 0, \\
&B + CO_{2d} - IC = 0, \\
&B + S^- - Z = 0,
\end{aligned}
\tag{4}
$$

where S^- is ionized acetic acid (mol L^{-1}), H^+ ionized hydrogen (mol L^{-1}), B measured bicarbonate (mol L^{-1}), Z the total of cations (mol L^{-1}), CO_{2d} dissolved carbon dioxide (mol L^{-1}), K_a is an acid-base equilibrium constant, K_b is an equilibrium constant between B and CO_{2d}. Finally, the gaseous phase (CH_4 and CO_2) is considered as the process output:

$$
y = Y_{CH_4} + Y_{CO_2}
\tag{5}
$$

with:

$$
Y_{CH_4} = R_1 R_2 \mu_2 X_2
\tag{6}
$$

$$
Y_{CO_2} = \lambda R_2 R_3 \mu_2 X_2
\tag{7}
$$

λ is defined as:

$$
\lambda_k = \frac{CO_{2d}}{P_t K_h - CO_{2d}}
\tag{8}
$$

where P_t is atmospheric pressure (Pa), K_h is a gases Henry constant (mol L^{-1} Pa^{-1}) and CO_{2d} defined as before. Biomass growth and substrate degradation are good indicators of CH_4 production [41] and biological activity inside the reactor. These variables can be used for monitoring the process and to design an inverse optimal neural control.

2.2   Recurrent neural networks

Recurrent neural networks are different from feedforward ones, because they have at least one feedback loop. This recurrent structure has a large impact on the learning capability of the network and on its performance [14], [42], [43]. This structure also offers a better suited tool to model and control nonlinear systems [15]. Using neural networks, control algorithms can be developed to be robust to uncertainties and modeling errors [44], [45], [46], [47]. RHONN are a generalization of the first-order Hopfield networks; they are proposed in [16]. RHONN are efficient for modeling, identification and control of complex nonlinear dynamic systems.

2.2.1   Recurrent high order neural observer design

A nonlinear discrete-time recurrent high order neural observer (RHONO) for unknown nonlinear systems in presence of external disturbances and parameter uncertainties is described in [48]. This observer is based on a discrete-time recurrent high-order neural network (RHONN) trained with an EKF based algorithm. First, let consider the next nonlinear system, which is assumed to be observable:

$$
\begin{aligned}
x_{k+1} &= F\left(x_k, u_k\right) + d_k, \\
y_k &= h\left(x_k\right),
\end{aligned}
\tag{9}
$$

where $x_{k+1} \in R^n$ is the state vector of the system, $u_k \in R^m$ is the input vector, $y_k \in R^p$ is the output vector, $h(x_k) \in R^{p \times n}$ is a nonlinear function of the system states, $d_k \in R^n$ is a disturbance vector and $F(\cdot)$ is a smooth vector field; hence (9) can be also expressed component wise as:

$$
\begin{aligned}
x_{i,k+1} &= F_i\left(x_k, u_k\right) + d_{i,k}, \qquad i = 1,\ldots,n, \\
x_k &= \left[x_{1,k}\ldots x_{i,k}\ldots x_{n,k}\right]^T, \\
d_k &= \left[d_{1,k}\ldots d_{i,k}\ldots d_{n,k}\right]^T, \\
y_k &= h\left(x_k\right).
\end{aligned}
\tag{10}
$$

For system (10), a *Luenberger-like* neural observer is proposed, with the following structure:

$$
\begin{aligned}
\hat{x}_k &= \left[\hat{x}_{1,k}\ldots\hat{x}_{i,k}\ldots\hat{x}_{n,k}\right]^T, \\
\hat{x}_{i,k+1} &= w_i^T z_i\left(\hat{x}_k, u_k\right) + g_i e_k, \\
\hat{y}_k &= h\left(\hat{x}_k\right); \qquad i = 1,\ldots,n,
\end{aligned}
\tag{11}
$$

with $g_i \in R^p$, u_i is the external input vector to the NN and z_i is a function of states and inputs to each neuron; the weight vectors are updated on-line with a decoupled EKF. The output error is defined as:

$$
e_k = y_k - \hat{y}_k.
\tag{12}
$$

The weight estimation error is defined as

$$
\tilde{w}_{i,k} = w_{i,k} - w_i^*
\tag{13}
$$

where w_i^* is the ideal weights vector and w_i its estimate.

The general DT nonlinear system (9), which is assumed to be observable, can be approximated by the following DT RHONN parallel representation:

$$x_{i,k+1} = w_i^{*T} z_i\left(x_k, u_k\right) + \in_{z_i}, \quad i = 1, \ldots, n \tag{14}$$

where ϵ_{zi} is a bounded approximation error, which can be reduced by increasing the number of the adjustable weights. Assume that there exists ideal unknown weights vector w_i^* such that $\| \epsilon_{zi} \|$ can be minimized on a compact set $\Omega zi \subset R^{Li}$ The ideal weight vector w_i^* is an artificial quantity required only for analytical purposes and is defined as

$$w_i^* = \underset{w_i}{\arg\min} \left\{ \underset{x,u}{\sup} \left| F_i\left(x_k, u_k\right) - w_i^T z_i\left(\bullet\right) \right| \right\} \tag{15}$$

which is assumed to be unknown, and it constitutes the optimal set which renders the minimum approximation error, defined as ϵ_{zi}; $F_i(\bullet)$ is the ith component of $F(\bullet)$ [49].

Due to this fact, we use $w_{i,k}$ as the approximation of the weight vector w_i^* and ϵ_{zi}, the modelling error, corresponds to $w_i^* \neq w_{i,k}$. The estimate w_i is used for stability analysis which will be discussed later. Since w_i^* is constant, then

$$\tilde{w}_{i,k+1} - \tilde{w}_{i,k} = w_{i,k+1} - w_{i,k} \quad \forall k \in 0 \cup Z^+ \tag{16}$$

The weight vectors are updated on-line with a decoupled EKF.

The state observer $\tilde{x}_{i,k}$ error is stated as

$$\tilde{x}_{i,k} = x_{i,k} - \hat{x}_{i,k}. \tag{17}$$

The dynamics of $x_{i,k+1}$ can be expressed as

$$\tilde{x}_{i,k+1} = x_{i,k+1} - \hat{x}_{i,k+1}. \tag{18}$$

Then

$$\tilde{x}_{i,k+1} = w_{i,k}^{*T} z_i\left(x_k, u_k\right) + \in_{z_i} - w_{i,k}^T z_i\left(\hat{x}_k, u_k\right) - g_{mi} e_k. \tag{19}$$

Adding and subtracting $w_{i,k}^{*T} z_i\left(\hat{x}_k, u_k\right)$, it can be written as

$$x_{i,k+1} = \tilde{w}_{i,k} z_i\left(x_k, u_k\right) + \in'_{z_i} - g_i e_k \tag{20}$$

with

$$\epsilon'_{z_i} = w^{*T}_{i,k} z_i \left(\tilde{x}_k, u_k \right) + \epsilon_{z_i}$$
$$z_i \left(\tilde{x}_k, u_k \right) = z_i \left(x_k, u_k \right) - z_i \left(\hat{x}_k, u_k \right) \tag{21}$$

The dynamics of the weights vector estimation error is

$$\tilde{w}_{i,k+1} = \tilde{w}_{i,k} - \eta K_{i,k} e_k \tag{22}$$

Stability analysis for system (9) – (22) is presented in **[50]**. In Figure 5, the proposed observer scheme is displayed.
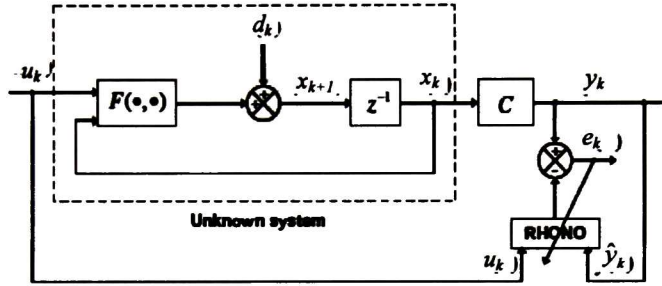
Figure 5 Observer scheme

where k is a real number representing a time sample, $x_k \in R^n$ is the state vector, $u_k \in R^m$ the input vector, $y_k \in R^p$ the output vector, $d_k \in R^n$ a disturbance vector, e_k the output error and $F(\cdot, \cdot)$ a smooth vector field.

2.2.2   EKF training algorithm

EKF based algorithms have been introduced to train neural network improving learning convergence. Since the neural network mapping is nonlinear, an EKF-type is required. The training goal is to find the optimal weight values, which minimize the predictions error. More details are presented in **[51]**, **[52]**. An EKF-based training algorithm is described by (23).

$$w_{i,k+1} = w_{i,k} + \eta_i K_{i,k} e_{i,k},$$
$$K_{i,k} = P_{i,k} H_{i,k} M_{i,k},$$
$$P_{i,k+1} = P_{i,k} - K_{i,k} H^T_{i,k} P_{i,k} + Q_{i,k}, \tag{23}$$
$$i = 1,...,n,$$

with:

$$M_{i,k} = \left[R_{i,k} + H^T_{i,k} P_{i,k} H_{i,k} \right]^{-1}$$
$$e_{i,k} = y_k - \hat{y}_k,$$

where $e_{i,k} \in R^P$ is the observation error, $P_{i,k} \in R^{LixLi}$ is the state prediction error associated covariance matrix at step k, $w_{i,k} \in R^{Li}$ is the weight (state) vector, L_i is the total number of neural network weights, $y \in R^P$ is the measured output vector, $\hat{y} \in R^P$ is the NN output, η_i is the learning rate parameter, $K_{i,k} \in R^{LixP}$ is the Kalman gain matrix, $Q_{i,k} \in R^{LixLi}$ is the state noise associated covariance matrix, $R_{i,k} \in R^{PxP}$ is the measurement noise associated covariance matrix, and $H_{i,k} \in R^{LixP}$ is a matrix for which each entry (H_{ij}) is the derivative of the i-th neural output with respect to ij-th NN weight, (w_{ij}). Where $i = 1, ..., n$ and $j = 1, ..., L_i$. Usually P_i, Q_i and R_i are initialized as diagonal matrices, with entries $P_{i,0}$, $Q_{i,0}$ and $R_{i,0}$ respectively. It is important to remark that $H_{i,k}$, $K_{i,k}$ and $P_{i,k}$ for the EKF are bounded [53].

2.2.3   Tuning guidelines

As discussed in [14], for NN learning P_i, Q_i and R_i can be selected and initialized as diagonals. The covariance matrices also verify:

$$P_{i,0} > R_{i,0} > Q_{i,0}. \tag{24}$$

This condition implies that a priori knowledge is not required to initialize the vector weights. In fact, higher entries in $P_{i,0}$ correspond to a higher uncertainty in the a priori knowledge. It is advisable to set $P_{i,0}$ between 100–1000 and so on for the other covariance matrices satisfying (24). An arbitrary scaling can be applied to $P_{i,0}$, $R_{i,0}$ and $Q_{i,0}$ without altering the evolution of the weight vector. As aforementioned, since the NN outputs do not depend directly on the weight vector, the matrix H is initialized as $H_0 = 0$. It is assumed that the weights values are initialized to small random values with zero mean and normal distribution. The learning rate (η) determines the magnitude of the correction term applied to each neuron weight; it is usually bounded as $0 < \eta < 1$. Thus, if η is small then the transient estimated state is over-damped; if η is large then the transient estimated state is under-damped; finally if η is larger than a critical value then the estimated state is unstable. Therefore, it is better to set η to a small value and to increase it if necessary. More details are discussed in [54].

2.3   Speed-gradient inverse optimal control

On this section, a speed-gradient-based inverse optimal control approach is presented for asymptotic stabilization of discrete-time nonlinear systems. A DT CLF in a quadratic form adjusted by means of the speed gradient algorithm is established for: a) to avoid the solution of the Hamilton-Jacobi-Bellman (HJB) equation and, b) to minimize a cost function. The proposed stabilizing optimal control uses the speed-gradient algorithm in order to determine the stabilizing control law. Thus, the combined approach is referred to as the speed-gradient inverse optimal control [31].

2.3.1 Optimal control

This section is devoted to briefly discuss the optimal control methodology and their limitations [30], [31].

Consider the affine-in-the-input discrete-time nonlinear system:

$$x_{k+1} = f(x_k) + g(x_k)u_k \tag{25}$$

where $x \in R^n$ is the state of the system, $u \in R^m$ is the control input, $f(x_k)$ and $g(x_k)$ are smooth maps with $f(x_k) \in R^n$, $g(x_k) \in R^{n \times m}$, subscript $k \in Z^+ \cup 0$ is the k-th sample k. We consider that x is an isolated fixed point of $f(x_k) + g(x_k)\bar{u}$ with $\bar{u}$ constant, that is, $f(\bar{x}) + g(\bar{x})\bar{u} = \bar{x}$. Without loss of generality, we consider $\bar{x} = 0, f(0) = 0$ and $rank\{g(x)\} = m \; \forall x_k \neq 0$.

The following cost functional is associated with system (25):

$$V(z_k) = \sum_{n=k}^{\infty} \left(l(z_n) + u_n^T R_C(z_n) u_n \right) \tag{26}$$

where $z_k = x_k - x_{\delta,k}$ with $x_{\delta,k}$ as the desired trajectory for x_k; $z_k \in R^n$; $V(z_k) : R^n \rightarrow R^+$; $l(z_k) : R^n \rightarrow R^+$ is a positive semidefinite function and $R_C(z_k) : R^n \rightarrow R^{m \times m}$ is a real symmetric positive definite weighting matrix. The cost functional (26) is a performance measure [55]. The entries of $R_C(z_k)$ can be functions of the system state in order to vary the weighting on control efforts according to the state value [55]. Considering state feedback control, we assume that the full state x_k is measurable. Then, (26) can be rewritten as

$$\begin{aligned} V(z_k) &= l(z_k) + u_k^T R_C(z_k) u_k \\ &\quad + \sum_{n=k+1}^{\infty} \left(l(z_n) + u_n^T R_C(z_n) u_n \right) \\ &= l(z_k) + u_k^T R_C(z_k) u_k + V(z_{k+1}) \end{aligned} \tag{27}$$

where we require the boundary condition $V(0) = 0$ so that $V(z_k)$ becomes a Lyapunov function.

From Bellman's optimality principle [56], [57], it is known that, for the infinite horizon optimization case, the value function $V(z_k)$ becomes time invariant and satisfies the DT Bellman equation [58], [59]

$$V(z_k) = \min_{u_k} \left\{ l(z_k) + u_k^T R(z_k) u_k + V(z_{k+1}) \right\} \tag{28}$$

where $V(z_{k+1})$ depends on both z_k and u_k. Note that the DT Bellman equation is solved backward in time [58]. In order to establish the conditions that the optimal control law must satisfy, we define the discrete-time Hamiltonian H [60] as

$$H(z_k, u_k) = l(z_k) + u_k^T R_C(z_k) u_k + V(z_{k+1}) - V(z_k) \tag{29}$$

A necessary condition that the optimal control law u_k should satisfy is $\partial H / \partial u_k = 0$ [55], which is equivalent to calculate the gradient of (28) right-hand side with respect to u_k, then

$$0 = 2R_C(z_k) u_k + \frac{\partial V(z_{k+1})}{\partial u_k} \tag{30}$$

$$= 2R_C(z_k) u_k + \frac{\partial z_{k+1}}{\partial u_k} \frac{\partial V(z_{k+1})}{\partial z_{k+1}} \tag{31}$$

$$= 2R_C(z_k) u_k + g^T(x_k) \frac{\partial V(z_{k+1})}{\partial z_{k+1}} \tag{32}$$

Therefore, the optimal control law is formulated as

$$u_k^* = -\frac{1}{2} R^{-1}(z_k) g^T(x_k) \frac{\partial V(z_{k+1})}{\partial x z_{k+1}}. \tag{33}$$

with the boundary condition $V(0) = 0$; u_k^* is used to emphasize that u_k is optimal. Moreover, if H has a quadratic form in u_k and $R(x_k) > 0$, then

$$\frac{\partial^2 H(x_{k+1})}{\partial u_k^2} > 0 \tag{34}$$

holds as a sufficient condition such that optimal control law (33) globally [55] minimizes H and the performance index (26) [57]. Substituting (33) into (28), we obtain

$$l(z_k) + V(z_{k+1}) - V(z_k) + \frac{1}{4} \frac{\partial V^T(z_{k+1})}{\partial z_{k+1}} g(x_k) R^{-1}(z_k) g^T(x_k) \frac{\partial V(z_{k+1})}{\partial z_{k+1}} = 0 \tag{35}$$

Solving the HJB partial-differential equation (35) for $V(z_k)$ is not straightforward. This is one of the main disadvantages in discrete-time optimal control for nonlinear systems. To overcome this problem, we propose to solve the inverse optimal control problem.

2.3.2 Lyapunov Stability

Due to the fact that the inverse optimal control is based on a Lyapunov function, we establish the following definitions.

Definition 1. Radially Unbounded Function [61]. A function $V(z_k)$ satisfying the condition

$V(z_k) \to \infty$ as $\|x_k\| \to \infty$ is said to be radially unbounded.

Definition 2. Control Lyapunov Function [62]. Let $V(z_k)$ be a radially unbounded function, with $V(z_k) > 0$, $\forall z_k \neq 0$ and $V(0) = 0$. If for any $z_k \in R^n$, there exist real values u_k such that

$$\Delta V(z_k) < 0 \tag{36}$$

where the Lyapunov difference $\Delta V(z_k)$ is defined as $V(z_{k+1}) - V(z_k)$. Then $V(\cdot)$ is said to be a "discrete-time control Lyapunov function" (CLF) for system (25).

Theorem 1. Asymptotic Stability [63]: The equilibrium $x_k = 0$ of (25) is globally asymptotically stable if there is a function $V(z) : R^n \to R$ such that

    (i) V is a positive definite function, decrescent and radially unbounded, and

    (ii) $-\Delta V(z_k)$ is a positive definite function.

2.3.3 Inverse Optimal Control

Definition 3. Inverse Optimal Control Law.
Let define the control law

$$u_k^* = -\frac{1}{2} R^{-1}(z_k) g^T(x_k) \frac{\partial V(z_{k+1})}{\partial z_{k+1}} \tag{37}$$

to be inverse optimal (globally) stabilizing along the desired trajectory $x_{\delta,k}$ if:

    (i)   it achieves (global) asymptotic stability of $x_k = 0$ for system (25) along reference $x_{\delta,k}$;

    (ii) $V(z_k)$ is (radially unbounded) positive definite function such that inequality

$$\overline{V} := V(z_{k+1}) - V(z_k) + u_k^{*T} R(z_k) u_k^* \leq 0 \tag{38}$$

is satisfied. When $l(z_k) := \overline{V}$, then $V(z_k)$ is a solution for (35) and cost functional (26) is minimized.

As is established in Definition 3, the inverse optimal control problem is based on the knowledge of $V(z_k)$. Then, a CLF $V(z_k)$ is proposed such that *(i)* and *(ii)* are guaranteed. Hence, instead of solving (35) for $V(z_k)$, we propose a CLF $V_c(z_k)$ with the form:

$$V_c(z_k) = \frac{1}{2} z_k^T P_k z_k \qquad P_k = P_k^T > 0 \tag{39}$$

Moreover it will be established that the control law (37) with (39), which is referred to as the inverse optimal control law, optimizes a cost functional of the form (26). This will be achieved by defining an appropriate matrix P_k. Consequently, by considering $V_c(z_k)$, the control law (37) takes the following form:

$$
\begin{aligned}
u_k^* &= -\frac{1}{4} R^{-1}(z_k) g^T(x_k) \frac{\partial z_{k+1}^T P_k z_{k+1}}{\partial z_{k+1}} \\
&= -\frac{1}{2} R^{-1}(z_k) g^T(x_k) P_k z_{k+1} \\
&= -\frac{1}{2}\left(R(z_k) + \frac{1}{2} g^T(x_k) P_k g(x_k) \right)^{-1} g^T(x_k) P_k \left(f(x_k) - x_{\delta,k+1} \right).
\end{aligned}
\tag{40}
$$

It is worth to point out that P_k and $R(z_k)$ are positive definite and symmetric matrices; thus, the existence of the inverse in (40) is ensured. To compute P_k, which guarantees trajectory tracking of x_k for system (25) with (40), along the desired trajectory $x_{\delta,k}$ we will use the speed-gradient (SG) algorithm.

2.3.4 Speed-gradient algorithm

In [64] DT application of the SG algorithm is formulated as finding a control law u_k which ensures the control goal:

$$
Q(z_{k+1}) \leq \Delta, \qquad for\ k \geq k^*
\tag{41}
$$

where Q is a control goal function, a constant $\Delta > 0$, and $k^* \in Z^+$ is the time step at which the control goal is achieved. Q ensures stability if it is a positive definite function.

Control law (40) at every time step depends on the matrix P_k. Let define this matrix P_k as:

$$
P_k = p_k P_C
\tag{42}
$$

where $P_C = P_C^T > 0$ is a given constant matrix of appropriate dimensions and p_k is a scalar parameter to be adjusted by the SG algorithm. Then, (40) is transformed into:

$$
u_k = -\frac{p_k}{2}\left(R(z_k) + \frac{p_k}{2} g^T(x_k) P_C g(x_k) \right)^{-1} g^T(x_k) P_C \left(f(x_k) - x_{\delta,k+1} \right)
\tag{43}
$$

The SG algorithm is now reformulated for the trajectory tracking inverse optimal control problem.

Definition 4. SG goal function for trajectory tracking

Consider a time-varying parameter $p_k \in P \subset R^+$ with $p_k > 0$ for all k, and P is the set of admissible values for p_k.

A nonnegative C^l function $Q: R^n \times R \rightarrow R$ of the form

$$Q(z_k, p_k) = V_{SG}(z_{k+1}),\tag{44}$$

where $V_{SG}(z_{k+1}) = \frac{1}{2} z_{k+1}^T P_C z_{k+1}$ is referred to as SG goal function for system (25), control law (43) and

desired reference $x_{\delta,k+1}$.

Definition 5. SG Control goal

Consider a constant $p^* \in P$. The SG control goal for system (25) with (43) is defined as finding p_k so that the SG goal function $Q_k(p)$ as defined in (44) fulfills:

$$Q_k(p) \leq \Delta(z_k), \text{ for } k \geq k^*\tag{45}$$

where

$$\Delta(z_k) = V_{SG}(z_k) - \frac{1}{p_k} u_k^T R(z_k) u_k\tag{46}$$

with $V_{SG}(z_k) = \frac{1}{2} z_k^T P_C z_k$ and u_k as defined in (43); $k^* \in Z^+$ is the time at which the SG control goal is

achieved.

Solution p_k must ensure that $V_{SG}(z_k) > \frac{1}{p_k} u_k^T R(z_k) u_k$ in order to obtain a positive definite function

$\Delta(z_k)$. The SG algorithm is used to compute p_k in order to achieve the SG control goal defined above.

Proposition 1. Consider a discrete-time nonlinear system of the form (25) with (43) as input. Let Q be a SG goal function as defined in (44) and denoted by $Q_k(p)$. Let $\bar{p}$, $p^* \in P$, be positive constant values and $\Delta(z_k)$ be a positive definite function with $\Delta(0) = 0$ and ϵ^* be a sufficiently small positive constant.

Assume that:

There exist p^* and ϵ^* such that

$$Q_k(p^*) \leq \epsilon^* << \Delta(z_k) \quad \text{and} \quad 1 - \epsilon^*/\Delta(z_k) \approx 1.\tag{47}$$

for all $p_k \in P$:

$$(p^* - p_k)^T \nabla_p Q_k(p) \leq \epsilon^* - \Delta(z_k) < 0\tag{48}$$

where $\nabla_p Q_k(p)$ denotes the gradient of $Q_k(p)$ with respect to p_k.

Then, for any initial condition $p_0 > 0$, there exists a $k^* \in Z^+$ such that the SG Control Goal (45) is achieved by means of the following dynamic variation of parameter p_k:

$$p_{k+1} = p_k - \gamma_{d,k} \nabla_p Q_k(p),\tag{49}$$

with

$$\gamma_{d,k} = \gamma_c \delta_k \left| \nabla_p Q_k(p) \right|^{-2} \qquad 0 < \gamma_c \le 2\Delta(z_k) \tag{50}$$

and

$$\delta_k = \begin{cases} 1 & for \quad Q(p_k) > \Delta(z_k) \\ 0 & otherwise. \end{cases} \tag{51}$$

Finally, for $k \ge k^*$, p_k becomes a constant value denoted by $\bar{p}$ and the SG algorithm is completed. Proof of this proposition is in [31].

Parameter γ_c in (50) is selected such that solution p_k ensures the requirement $V_{SG}(z_k) > \dfrac{1}{p_k} u_k^T R(z_k) u_k$. Then, we have a positive definite function $\Delta(z_k)$.

When SG Control Goal (45) is achieved, then $p_k = \bar{p}$ for $k \ge k^*$. Thus, matrix P_k in (40) is considered constant and $P_k = P_g$ where P_g is computed as $P_g = \bar{p}P_C$, with P_C a design positive definite matrix. Under these constraints, we obtain:

$$u_k^* = -\frac{1}{2}\left(R(z_k) + \frac{1}{2} g^T(x_k) P_g g(x_k) \right)^{-1} g^T(x_k) P_g \left(f(x_k) - x_{\delta,k+1} \right). \tag{52}$$

The proof that control law (52) ensures stability and optimality for (25) without solving the HJB equation (35) is presented in [31]. The control law (52) is inverse optimal in the sense that it minimizes the cost functional given by

$$J(z_k) = \sum_{k=0}^{\infty} \left(l(z_k) + u_k^T R(z_k) u_k \right) \tag{53}$$

where

$$l(z_k) := -\bar{V} \tag{54}$$

with $\bar{V}$ defined as

$$\bar{V} := V(z_{k+1}) - V(z_k) + u_k^T R(z_k) u_k. \tag{55}$$

Chapter 3

Neural observer synthesis and validation

This chapter discusses the observer structure for methanogenesis state estimation and the dynamic learning rate as a function of the pH substrate in order to improve the performance of the observer. The observer validation in presence of disturbances and parameter variations is presented via simulation and experimentally.

3.1 Neural observer for an anaerobic process

A nonlinear discrete-time neural observer (RHONO) is designed in order to estimate biomass concentration, substrate concentration and inorganic carbon for an anaerobic process. The training of the RHONO is performed on-line. The variables are estimated from CH_4 and CO_2 flow rates, which are commonly measured in this process. In addition, is assumed that pH and the process inputs are on-line measured. In most process these variables are easily measured.

3.1.1 Background

In order to design discrete-time RHONO, model (1)-(8) is discretized by Euler approximation, as follows. Consider the next nonlinear system:

$$\dot{x} = f(x) + g(x)u + d(t) \tag{56}$$

where $x \in R^n$ is the state of the system, $f(x): R^n \rightarrow R^n$ and $g(x): R^{n \times m} \rightarrow R^n$ are nonlinear functions, $u \in R^m$ is the control input, $d(t) \in R^n$ is a disturbance term. Discretization by Euler method is defined as:

$$x_{k+1} = x_k + T\left(f(x_k) + g(x_k)u_k + d_k\right), \tag{57}$$

where $k \in Z^+ \cup 0$ is the sampling time and T is discretization step.

By applying the Euler discretization method to the system (1)-(8), the next model is obtained:

$$
\begin{aligned}
X_{1,k+1} &= X_{1,k} + T\left(\left(\mu_{1,k} - k_{d1}\right)X_{1,k}\right), \\
S_{1,k+1} &= S_{1,k} + T\left(-R_6\mu_{1,k}X_{1,k} + D_{in,k}\left(S_{1in,k} - S_{1,k}\right)\right), \\
X_{2,k+1} &= X_{2,k} + T\left(\left(\mu_{2,k} - k_{d2}\right)X_{2,k}\right), \\
S_{2,k+1} &= S_{2,k} + T\left(-R_3\mu_{2,k}X_{2,k} + R_4\mu_{1,k}X_{1,k} + D_{in,k}\left(S_{2in,k} - S_{2,k}\right)\right), \\
IC_{k+1} &= IC_k + T\left(R_2R_3\mu_{2,k}X_{2,k} + R_5\mu_{1,k}X_{1,k} - \lambda_k R_1R_3\mu_{2,k}X_{2,k} + D_{in,k}\left(IC_{in,k} - IC_k\right)\right), \\
Z_{k+1} &= Z_k + T\left(D_{in,k}\left(Z_{in,k} - Z_k\right)\right),
\end{aligned}
\tag{58}
$$

The gaseous phase (CH_4 and CO_2) considered as the process output is definite as:

$$
y_k = Y_{CH_4,k} + Y_{CO_2,k}
\tag{59}
$$

with:

$$
Y_{CH_4,k} = R_1 R_2 \mu_{2,k} X_{2,k}
\tag{60}
$$

$$
Y_{CO_2,k} = \lambda_k R_2 R_3 \mu_{2,k} X_{2,k}
\tag{61}
$$

This model is as described in (9). The observability property of this anaerobic digestion process is analyzed in a previous work [4], [10]. From this analysis is proven which Z_k is the unique non-observable state, however Z_k is biologically inert and its dynamic depends only on hydrodynamic behavior. Additionally, $S_{1,k}$ and $X_{1,k}$ are related to the fast stage and they are not considered for the observer design, because the main interest is on the slow one. Thus, a RHONO for the methanogenic stage is proposed.

3.1.2 Synthesis

The structure of RHONO, is formulated as

$$
\begin{aligned}
\hat{X}_{2,k+1} &= w_{11,k}S\left(\hat{X}_{2,k}\right) + w_{12,k}S^2\left(\hat{X}_{2,k}\right) + w_{13,k}S\left(\hat{IC}_k\right) \\
&\quad + w_{14,k}S^2\left(\hat{X}_{2,k}\right)D_{in,k} + w_{15,k}S^2\left(\hat{X}_{2,k}\right)b_{inc,k} + g_1 e_k, \\
\hat{S}_{2,k+1} &= w_{21,k}S\left(\hat{S}_{2,k}\right) + w_{22,k}S^2\left(\hat{S}_{2,k}\right) + w_{23,k}S\left(\hat{IC}_k\right) \\
&\quad + w_{24,k}S^2\left(\hat{S}_{2,k}\right)D_{in,k} + w_{25,k}S^2\left(\hat{S}_{2,k}\right)S_{2in,k} + g_2 e_k, \\
\hat{IC}_{k+1} &= w_{31,k}S\left(\hat{IC}_k\right) + w_{32,k}S^2\left(\hat{IC}_k\right) + w_{33,k}S\left(\hat{X}_{2,k}\right) \\
&\quad + w_{34,k}S^2\left(\hat{IC}_k\right)D_{in,k} + w_{35,k}S^2\left(\hat{IC}_k\right)b_{inc,k} + g_3 e_k,
\end{aligned}
\tag{62}
$$

where w_{ij} is the respective on-line adapted weight vector; $\hat{X}_{2,k}, \hat{S}_{2,k}$ and $\hat{IC}_k$ are the estimated states; $S(\bullet)$ is the sigmoid function defined as $S(x) = \alpha \tanh(\beta x)$; (g_1, g_2, g_3) are the Luenberger-like observer gains, e_k is the output error, b_{inc} is the bicarbonate input, $D_{in,k}$ and $S_{2in,k}$ are defined as in section 2.1.3.

The observer output is defined as follows:

$$\hat{y}_k = \hat{Y}_{CH_4,k} + \hat{Y}_{CO_2,k} \tag{63}$$

with:

$$\hat{Y}_{CH_4,k} = R_1 R_2 \hat{\mu}_{2,k} \hat{X}_{2,k} \tag{64}$$

$$\hat{Y}_{CO_2,k} = \hat{\lambda}_k R_2 R_3 \hat{\mu}_{2,k} \hat{X}_{2,k}. \tag{65}$$

The output error e_k is defined as:

$$e_k = y_k - \hat{y}_k \tag{66}$$

As shown in (62), the proposed neuronal observer has a parallel configuration and the vector of weights w_{ij} is on-line updated with the EKF given by (23). RHONO for AD process scheme is illustrated in Figure 6.
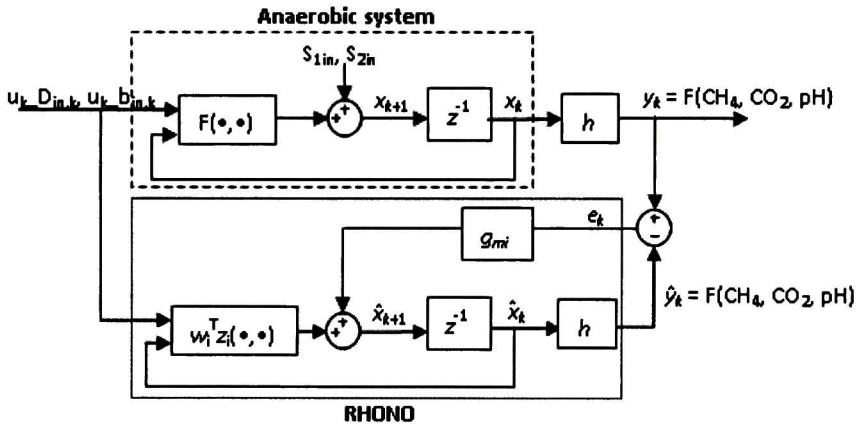
Figure 6 RHONO scheme for AD process

This scheme illustrates the inputs of the AD process $D_{in,k}$ and $b_{in,k}$, $x_k \in R^n$ represents the states of the system, $\hat{x}_k \in R^n$ the estimated states $\hat{X}_{2,k}, \hat{S}_{2,k}$ and $\hat{IC}_k$, $y_k \in R^p$ the measurable output of the system, $\hat{y}_k \in R^p$ is the estimated output of the observer, e_k the output error, $F(\cdot .\cdot)$ and $w_i^T z_i(\cdot .\cdot)$ are smooth vector fields.

3.1.3 Time-varying learning rate

Parameter η in the FKE determines the magnitude of the correction term applied to each neuron weight. This parameter is bounded and its value is selected heuristically as discussed in section 2.2.3. In previous works [28], [65] the use of constant values illustrates a good performance in presence of small disturbances; however it presents a transient error increase in presence of large disturbances for AD process. Values of this parameter can be selected heuristically in order to find the best performance.

One of the main contributions of this work is a methodology to obtain a time-varying learning rate (η_D), in order to enhance the performance of neuronal observers. η_D is proposed to be computed on-line as a function of the system operating conditions; this variable improves the learning of the neuronal network in presence of disturbances and parameter variations.

For the AD process η_D is calculated as a function of the pH substrate, which represents different system operating conditions. The pH is an important parameter for the adequate growth of bacteria and then for waste transformation. For methanogenesis, the optimal range of substrate pH is between 6 and 8. Bicarbonate ions and volatile fatty acids (VFA) concentration have an influence on the pH. A pH value higher than 8 causes an inhibition of the bacteria activity, while a value under 5 for a long time causes irreversible damaged and death of the bacteria, stopping the process due to acidification [4]. Therefore, considering that the pH is a sensible and determining variable in the process, it is used to determine η_D as proportional (γ) to the on-line measurement substrate pH, as presented in Figure 7.
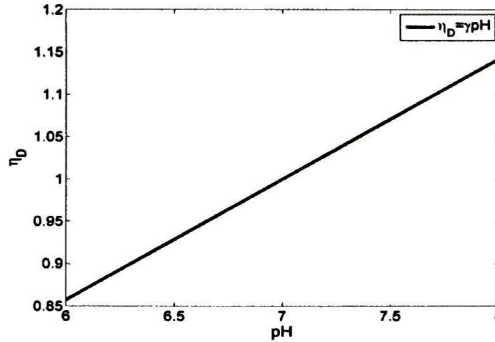

Figure 7 Time-varying learning rate as a function of pH

In order to implement a time varying learning rate, the EKF training algorithm (23) is modified as follows:

$$w_{i,k+1} = w_{i,k} + \eta_{Di,k} K_{i,k} e_{i,k}. \tag{67}$$

with $\left| \eta_{D_{i,k}} \right| < \delta$ and δ is function of the pH level (Figure 7). The other components of the algorithm remain unchanged.

Before to state the convergence analysis of the observer, let us recall the nonlinear system assumed observable as presented in section 2.2.1:

$$x_{k+1} = F(x_k, u_k) + d_k,$$
$$y_k = h(x_k), \tag{68}$$

with x_k, u_k, d_k, y_k, $h(x_k)$, and $F(\cdot)$ as defined before. For system (68) a *Luenberger-like* neural observer is proposed:

$$\hat{x}_k = \left[\hat{x}_{1,k}...\hat{x}_{i,k}...\hat{x}_{n,k}\right]^T$$
$$\hat{x}_{i,k+1} = w_i^T z_i(\hat{x}_k, u_k) + g_i e_k, \tag{69}$$
$$\hat{y}_k = h(\hat{x}_k); \qquad i = 1,...,n,$$

where $\hat{x}_k$, w_i, g_i, z_i and $\hat{y}_k$ are defined as before. The output error is expressed as:

$$e_k = y_k - \hat{y}_k. \tag{70}$$

The weight estimation error is defined as

$$\tilde{w}_{i,k} = w_{i,k} - w_i{}^* \tag{71}$$

where w_i^* is the ideal weights vector. The dynamics of the weights vector estimation error is

$$\tilde{w}_{i,k+1} = \tilde{w}_{i,k} - \eta K_{i,k} e_k. \tag{72}$$

The state observer $\tilde{x}_{i,k}$ error is stated as

$$\tilde{x}_{i,k} = x_{i,k} - \hat{x}_{i,k}, \tag{73}$$

which dynamic is expressed as

$$\tilde{x}_{i,k+1} = \tilde{w}_{i,k} z_i(x_k, u_k) + \epsilon'_{z_i} - g_{mi} e_k \tag{74}$$

with

$$\epsilon'_{z_i} = \epsilon_{z_i} + d_{i,k} \tag{75}$$

where ϵ_{zi} is a bounded approximation error. The convergence analysis is stated as the follows theorem.

Theorem 2: *For system (68), the RHONO (69), trained with the EKF-based algorithm (23) with $w_{i,k+1}$ determined as (67), ensures that the i-th (i = 1, 2, . . . , n) estimation error (73) and the output error (70) are semiglobally uniformly ultimately bounded (SGUUB); moreover, the RHONO weights remain bounded.*

Proof. Let assume that $h(\cdot)$ is a known output function which is Lipschitz in x_k,

$$\left\| h(x_k) - h(\hat{x}_k) \right\| \le L \left\| x_k - \hat{x}_k \right\| \tag{76}$$

with L the Lipschitz constant [61].

First, let consider the candidate Lyapunov function with P_{qi} a positive definite and symmetric matrix

$$V_{i,k} = \tilde{w}_{i,k} P_{qi,k} \tilde{w}_{i,k} + \tilde{x}_{i,k} P_{qi,k} \tilde{x}_{i,k} \tag{77}$$

whose first increment is defined as

$$
\begin{aligned}
\Delta V_{i,k} &= V_{k+1} - V_k \\
&= \tilde{w}_{i,k+1} P_{qi,k+1} \tilde{w}_{i,k+1} + \tilde{x}_{i,k+1} P_{qi,k+1} \tilde{x}_{i,k+1} - \tilde{w}_{i,k} P_{qi,k} \tilde{w}_{i,k} - \tilde{x}_{i,k} P_{qi,k} \tilde{x}_{i,k}
\end{aligned}
\tag{78}
$$

Using the EKF (23) and (71) in (78), then

$$
\begin{aligned}
\Delta V_{i,k} &= \left[\tilde{w}_{i,k} - \eta_{Di} K_{i,k} e_k \right]^T \left[A_{i,k} \right] \times \left[\tilde{w}_{i,k} - \eta_{Di} K_{i,k} e_k \right] + \left[f_k - g_i e_k \right]^T \left[A_{i,k} \right] \times \left[f_k - g_i e_k \right] \\
&\quad - \tilde{w}_{i,k} P_{qi,k} \tilde{w}_{i,k} - \tilde{x}_{i,k} P_{qi,k} \tilde{x}_{i,k}
\end{aligned}
\tag{79}
$$

with

$$
\begin{aligned}
A_{i,k} &= P_{qi,k} - D_{i,k} + Q_i \\
D_{i,k} &= K_{i,k} H_{i,k}^T P_{qi,k} \\
f_k &= \tilde{w}_{i,k} z_i (x_k, u_k) + \varepsilon'_{z_i}
\end{aligned}
$$

Hence, (79) can be expressed as

$$
\begin{aligned}
\Delta V_{i,k} &= 2\tilde{w}_{i,k}^T P_{qi,k} \tilde{w}_{i,k} - 2\tilde{w}_{i,k}^T \left[B_{i,k} \right] \tilde{w}_{i,k} + 2\eta_{Di}^2 e_k^T K^T \left[A_{i,k} \right] K_{i,k} e_k + 2 f_k^T A_{i,k} f_k \\
&\quad + 2 e_k^T g_i^T \left[A_{i,k} \right] g_i e_k - \tilde{w}_{i,k} P_{qi,k} \tilde{w}_{i,k} - \tilde{x}_{i,k} P_{qi,k} \tilde{x}_{i,k}
\end{aligned}
\tag{80}
$$

with $B_{i,k} = D_{i,k} - Q_i$.

Using the following inequalities

$$X^T X + Y^T Y \geq 2X^T Y$$
$$X^T X + Y^T Y \geq -2X^T Y \tag{81}$$
$$-\lambda_{\min}(P) X^2 \geq -X^T P X \geq -\lambda_{\max}(P) X^2$$

which are valid $\forall X, Y \in R^n, \forall P_{qi} \in R^{n \times n}, P_{qi} = P_{qi}^T > 0$, and considering (76), (80) can be rewritten as

$$\Delta V_{i,k} \leq \|\tilde{w}_{i,k}\|^2 \lambda_{\max}(P_{qi,k}) - \|\tilde{w}_{i,k}\|^2 \lambda_{\min}(B_{i,k}) + 2\|\tilde{x}_k\|^2 \|\delta K_i L\|^2 \lambda_{\max}(A_{i,k})$$
$$+ 2\|f_k\|^2 \lambda_{\max}(A_{i,k}) + 2\|\tilde{x}_k\|^2 \|g_i L\|^2 \lambda_{\max}(A_{i,k}) - \|\tilde{x}_k\|^2 \lambda_{\min}(P_{qi,k}) \tag{82}$$

Substituting $f_k = \tilde{w}_{i,k} z_i(x_k, u_k) + \varepsilon'_{z_i}$, in (82), then

$$\Delta V_{i,k} \leq \|\tilde{w}_{i,k}\|^2 \lambda_{\max}(P_{qi,k}) - \|\tilde{w}_{i,k}\|^2 \lambda_{\min}(B_{i,k}) + 2\|\tilde{x}_k\|^2 \|\delta K_i L\|^2 \lambda_{\max}(A_{i,k})$$
$$+ 4\|\varepsilon'_{z_i}\|^2 \lambda_{\max}(A_{i,k}) + 4\|\tilde{w}_{i,k}\|^2 \|z_i(x_k, u_k)\|^2 \lambda_{\max}(A_{i,k}) \tag{83}$$
$$+ 2\|\tilde{x}_k\|^2 \|g_i L\|^2 \lambda_{\max}(A_{i,k}) - \|\tilde{x}_k\|^2 \lambda_{\min}(P_{qi,k})$$

Defining

$$E_{i,k} = 2\|\delta K_i L\|^2 \lambda_{\max}(A_{i,k}) + 2\|g_i L\|^2 \lambda_{\max}(A_{i,k}) - \lambda_{\min}(P_{qi,k})$$
$$F_{i,k} = \lambda_{\max}(P_{qi,k}) - \lambda_{\min}(P_{qi,k}) + 4\|z_i(x_k, u_k)\|^2 \lambda_{\max}(A_{i,k})$$

Then (83) can be rewritten as

$$\Delta V_{i,k} \leq -\|\tilde{x}_k\|^2 E_{i,k} - \|\tilde{w}_{i,k}\|^2 F_{i,k} + 4\|\varepsilon'_{z_i}\|^2 \lambda_{\max}(A_{i,k}) \tag{84}$$

Hence $\Delta V_{i,k} \leq 0$ when

$$\|\tilde{x}_k\| > \sqrt{\frac{4\|\varepsilon'_{z_i}\|^2 \lambda_{\max}(A_{i,k})}{E_{i,k}}} \equiv k_{1,k}$$

or

$$\|\tilde{w}_{i,k}\| > \sqrt{\frac{4\|\varepsilon'_{z_i}\|^2 \lambda_{\max}(A_{i,k})}{F_{i,k}}} \equiv k_{2,k}$$

Therefore the solution of (72) and (74) is SGUUB; hence, the estimation error and the RHONO weights are SGUUB [66].

To proceed with the proof for all the states, let consider the Lyapunov function candidate.

$$V_k = \sum_{i=1}^{n} \left(\tilde{w}_{i,k} P_{qi,k} \tilde{w}_{i,k} + \tilde{x}_{i,k} P_{qi,k} \tilde{x}_{i,k} \right) \tag{85}$$

$$\Delta V_k = \sum_{i=1}^{n} \left(\tilde{w}_{i,k+1} P_{qi,k+1} \tilde{w}_{i,k+1} + \tilde{x}_{i,k+1} P_{qi,k+1} \tilde{x}_{i,k+1} - \tilde{w}_{i,k} P_{qi,k} \tilde{w}_{i,k} - \tilde{x}_{i,k} P_{qi,k} \tilde{x}_{i,k} \right) \tag{86}$$

Therefore, (85) can be expressed in the following equation

$$\Delta V_k \le \sum_{i=1}^{n} \left(-\|\tilde{x}_k\|^2 E_{i,k} - \|\tilde{w}_{i,k}\|^2 F_{i,k} + 4 \left| \varepsilon'_{z_i} \right|^2 \lambda_{max} \left(A_{i,k} \right) \right)$$

with E_i and F_i defined as above. Hence $\Delta V_{i,k} < 0$ when

$$\|\tilde{x}_k\| > k_{1,k}$$

or

$$\|\tilde{w}_{i,k}\| > k_{2,k}$$

If $\|\tilde{x}_k\| > k_{1,k}$ and $\|\tilde{w}_{i,k}\| > k_{2,k}, \forall i = 1,...,n$ holds, then $\Delta V_{i,k} < 0$.

Finally considering (69) and (70), it is easy to see that the output error has an algebraic relation with $\tilde{x}_k$; for that reason, if $\tilde{x}_k$ is bounded, then e_k is bounded too.

$$e_k = h \tilde{x}_k$$
$$\|e_k\| = \|h\| \|\tilde{x}_k\| \qquad \qquad \square$$

3.2 Observer validation via simulation

A set of simulations, close to real conditions, are presented to validate the proposed RHONO (62); the observer estimation convergence is tested at random initial conditions, in presence of disturbances on the input substrate and parameter variations in the growth rate. Parameter values are presented in Tables 1 and 2, appendix A. The process model and the observer are implemented using Matlab/Simulink™ (TM: The Mathworks Inc., Cambridge, MA, USA) in order to verify the performance of the RHONO via simulations.

First, constant values of η were determined in [13] for each one of the estimated variables as: $\eta_1=1$ for the estimation of X_2, $\eta_2=0.5$ for the estimation of S_2 and $\eta_3=10$ for the estimation of IC. The initial conditions for the observer states are presented in Table 2. A disturbance on the input substrate S_{2in} of 50% is incepted at t = 200 h in open loop, as shown in Figure 8.
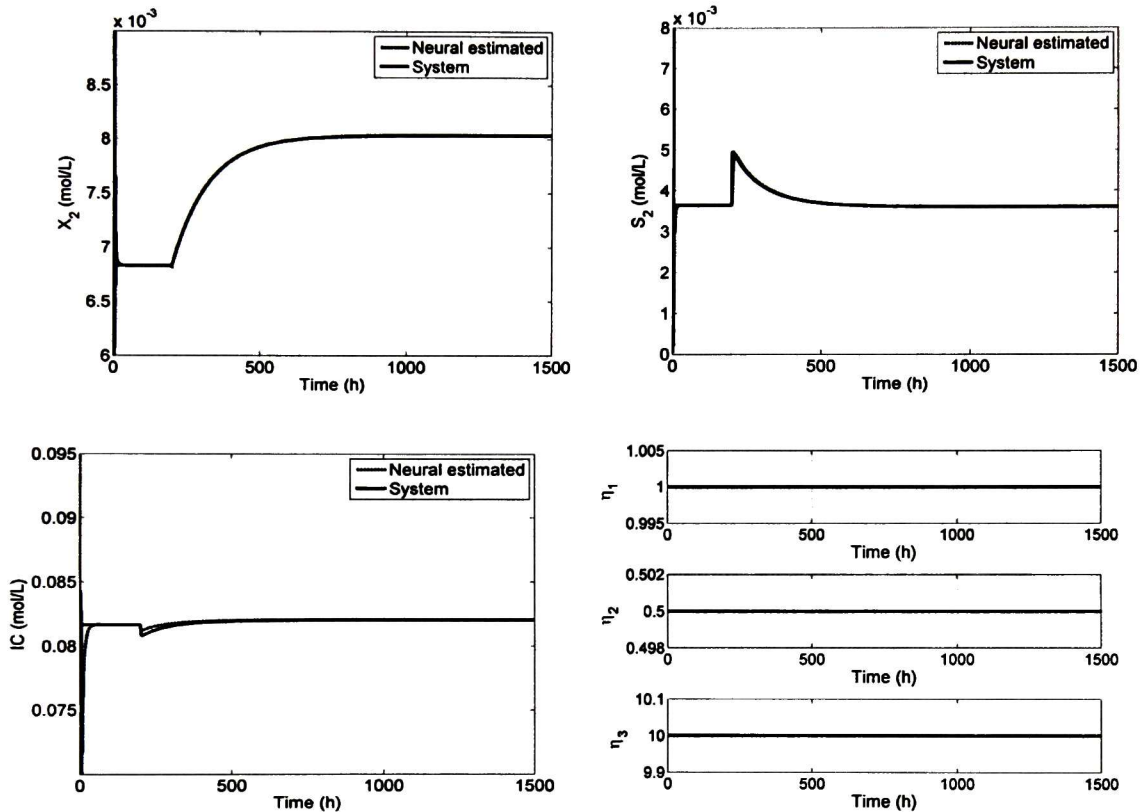
Figure 8 Estimated states with constant learning rate for test 1

As can be seen X_2, S_2 and IC are well estimated during all the simulation despite disturbance. Estimation presents a fast convergence from the beginning without transient error. Thus, the proposed neural observer trained with constant η_i for EKF-based algorithm is a good alternative to estimate those important system states. Figure 9 illustrates the disturbance in S_{2in} at $t=200$ h.
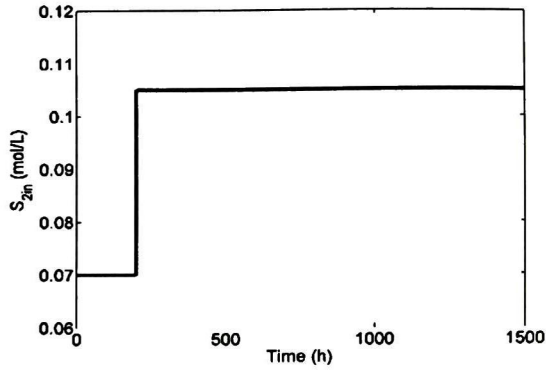
Figure 9 Input disturbance on the substrate

In order to show the performance improvement of the observer with a time-varying η_D, a comparative analysis between constant and time-varying learning rate is realized. AD system convergence is ensured in closed loop with a PID L/A controller designed in a previous work [65].

The second test is done with the following initial conditions for constant learning rate: $\eta_1 = 6.4$, $\eta_2 = 0.648$ and $\eta_3 = 20$. The initial conditions for the observer states are 40% smaller than the previous ones. On the other hand, observer tolerance to change on the system parameters is tested; such variation is incepted as a disturbance on the bacteria concentration, $\mu_{1max} = 0.0825$ and $\mu_{2max} = 0.023$. Parameter values are presented in Table 3, appendix A. Finally a disturbance on the input substrate S2in of 250% increase is incepted at t=200 h. Results are illustrated in Figure 10.


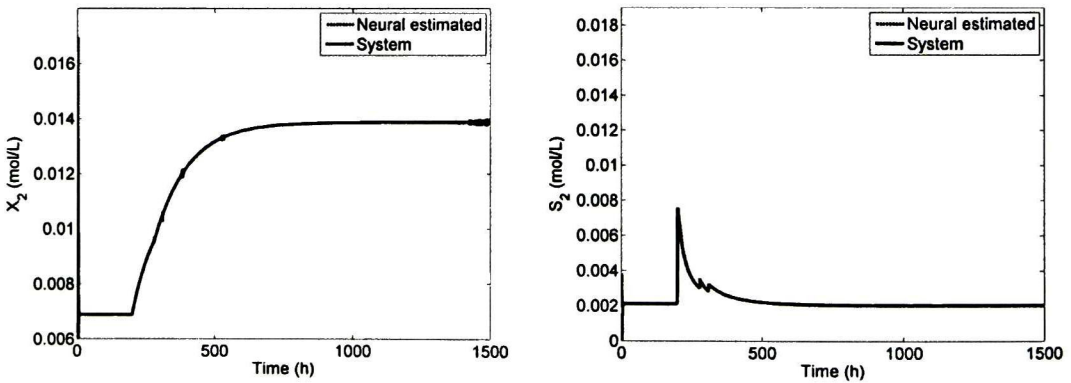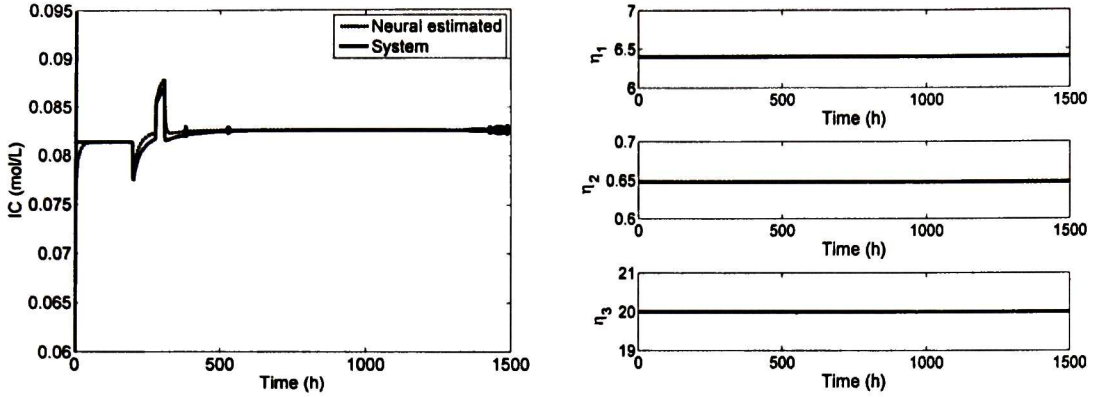**Figure 10 States estimation with constant learning rate for test 2**

Figure 10 (Continued)

Figure 10 illustrates the performance in closed loop of the observer and η_i trajectories when the disturbance on the input substrate is incepted. Observer presents a fast estimation convergence for all estates. As can be seen, $X_{2,k}$ is estimated with a transient error during all the simulation; particularly chattering in steady state is shown at the end of the simulation. This error could be due to disturbance amplitude which produces oscillations and the processor effect in the numerical simulation. A critical value exists for which the control cannot reject the disturbances and the system tends to washout. The IC_k estimation is similar as for the previous description. In contrast, $S_{2,k}$ is well estimated during all simulation. This behavior illustrates which the disturbance amplitude affects directly to the microorganisms and the pH related to the IC_k. Despite the errors in transient state and chattering, the observer is able to estimate adequately the three variables of methanogenesis stage.

Third test is done using time-varying η_{Di}, with the following initial conditions: $\eta_{D1} = 6.4$, $\eta_{D2} = 0.648$ and $\eta_{D3} = 20$. The other parameters of the neural observer remain unchanged.
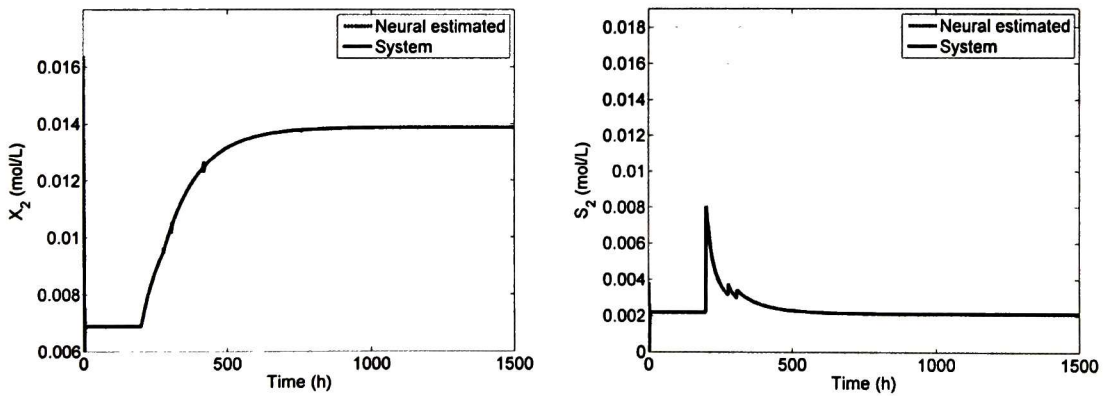

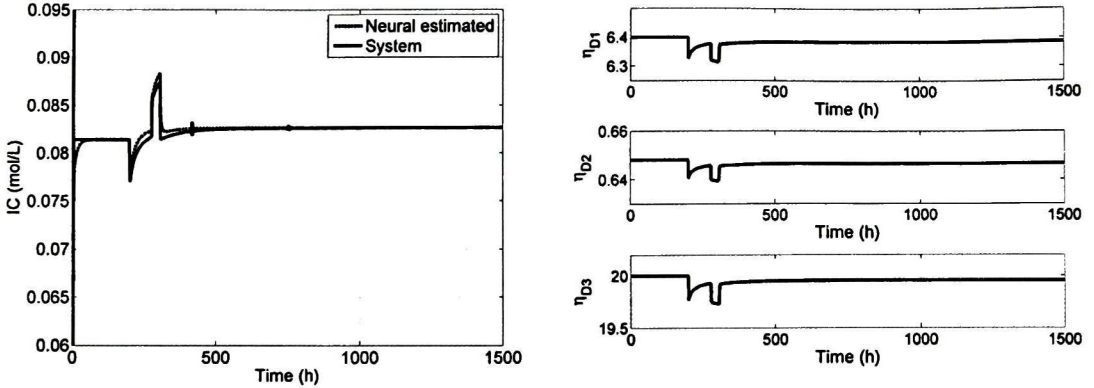**Figure 11 States estimation with time-varying learning rate for test 3**

Figure 11 (Continued)

Figure 11 illustrates the performance in closed loop of the observer and η_{Di}, when the disturbance on the input substrate is incepted. As can be seen with η_{Di}, transient state error of X_2 and IC states is decreased and chattering is eliminated as compared with Figure 10. S_2 remain well estimated. Therefore, from the simulation results, the η_{Di} contribute to better performance of the RHONO. Thus, the robustness of the proposed RHONO to parameters variations is verified.

The proposed neural observer trained with the EKF-based algorithm is a good alternative to estimate those important states in presence of disturbances on the input substrate, parameter variations on the growth rate and random initial conditions. The proposed η_D, as a function of the pH on-line measurement, produces good results.

3.3 Experimental validation

This section describes an experimental validation in order to verify the proposed neural observer performance in a laboratory scale wastewater treatment process. First, the experimental setup is presented and then the respective validation results.

3.3.1 Experimental setup

3.3.1.1 Biomass

Biomass is composed of anaerobic bacteria fixed as biofilm on a natural zeolite support which acts as a biomass filter. The substrate comes from an abattoir wastewater in Saltillo, Coahuila, Mexico as explained in [67]. Batch mode experiments are performed to obtain: bacteria adaptation to substrate and bacteria colonization on the zeolite.

Hydrodynamic behavior of the biomass filter allows obtaining high microorganisms concentration inside the reactor [67], which produces an efficient treatment of wastewater and improves methane production. In [68] a manure digestion study is presented, where biomass is immobilized on zeolite; use of the support produced a 59% and 35% increase in the values of growth rate and kinetic constant of the

process, respectively. This behavior is believed to be due to the exchange of ammoniacal nitrogen that occurs in this type of digester between the support and the medium. In [67] the effect of different sizes of zeolite particle is analyzed for an abattoir wastewater anaerobic treatment process. Natural zeolite of up to 1 mm (14 mesh) particle size was used in batch experiments. The anaerobic process was favored by the addition of natural zeolite at doses of between 0.05 and 0.30 g/g of volatile suspended solids. The significant contribution is the high capacity of zeolite for microorganisms immobilization. For this, a natural zeolite with 9-10 mesh particle size is used because this contributes to best biomass retention [67]. Deposited zeolite with bacteria biofilm at the bottom of the reactor is illustrated in Figure 12.
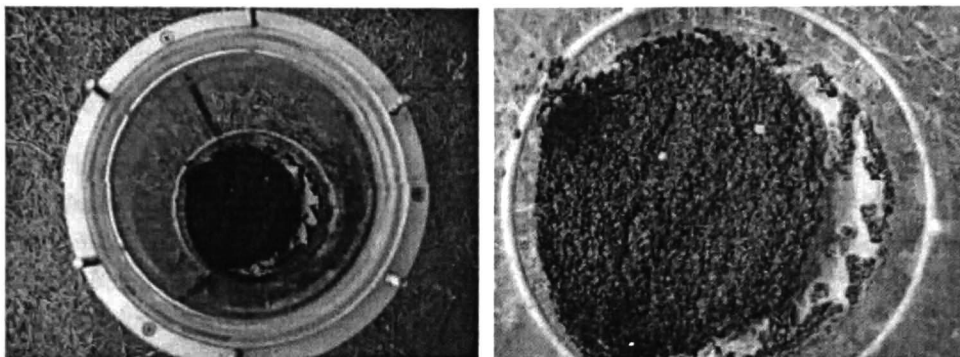
Figure 12 Bacteria colonization on natural zeolite

3.3.1.2   Substrate

Substrate samples are taken from an abattoir in Saltillo city, displayed in Figure 13; this abattoir has the TIF ("Tipo de Inspección Federal") federal certification, granted to meats processing plants which meet health and hygiene standards of the Mexican Government.

The abattoir effluents have a strong concentration of organic matter; typically contain a high concentration of proteins, fats, oils, suspended solids, other products of the meat industry and basic pH. Abattoir effluents within the food industry are classified as larger than 2000 mg L^{-1} [69]. Average composition on this wastewater type is shown in Table 4.

The mentioned effluents after solid residues separation go through an aerobic treatment process. A portion of the treated water is used for irrigation and the other part is integrated into the municipal water supply and sanitation [69].
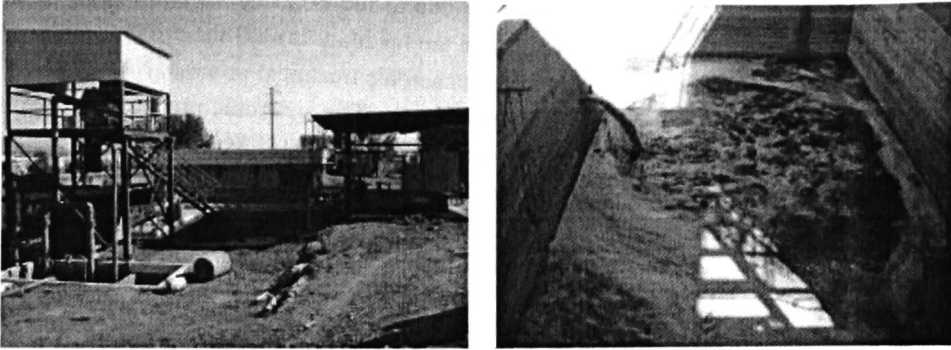
Figure 13 Municipal abattoir from Saltillo, Coahuila

3.3.1.3　Bioreactor

The employed CSTR is a laboratory prototype *Applikon®*; this system is composed of the following elements: bioreactor with capacity of 7 L, featuring a metallic lid to seal it hermetically, in which are located the pH sensor, temperature sensor, dissolved O_2 sensor, liquid level and agitation speed; ADI 1010 controller, for the regulation of variables such as pH, temperature, dissolved O_2, liquid level and agitation speed; ADI 1025 console, which consists of the actuators for the variables regulation, as feeding and substrate extraction pumps, transfer heat, base addition, etc. Databases of the pH and temperature variables are obtained using the BioXpert Lite® data acquisition system.

A bioreactor configuration is illustrated in Figure 14.
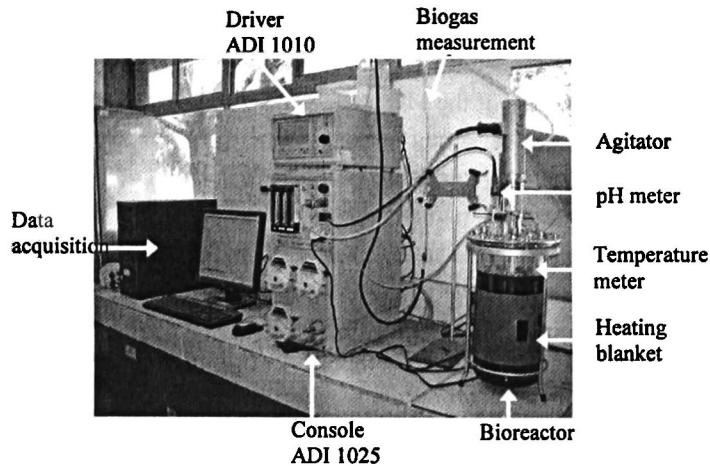
Figure 14 Bioreactor configuration

3.3.1.4　Measurement of variables

The experiment is performed in a prototype bioreactor of 7 L (Figure 14) as follows: a continuous configuration is used considering an input flow rate (Q_{in}) of 450 mL h^{-1}, D_{in} of 0.1 h^{-1}, substrate volume of 4.5 L, 400 mg of zeolite, constant temperature of 37 °C, initial pH of 6.85 and agitation speed of 100 rpm. Continuous configuration is operates during ten days after bacteria adaptation. During this test, the next

variables are measured [70]: pH, biogas, input substrate COD (chemical oxygen demand) and output substrate COD. Data Measured are illustrated in Figure 15.
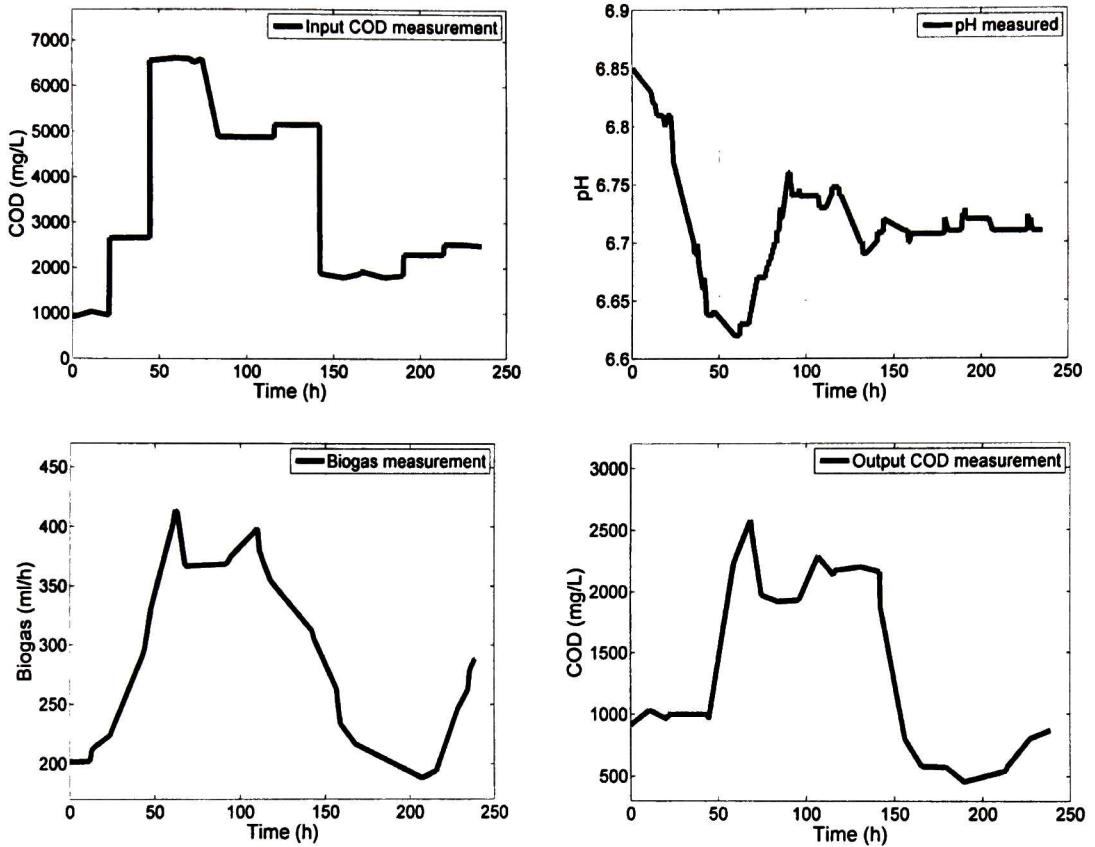
Figure 15 Variables measurement

To keep constant the reactor volume, the input and output flow rates are controlled independently by means of pumps. The prototype is equipped with sensors to measure temperature and pH inside the reactor. A homogeneous environment is assured inside the reactor by a stirring system. The produced biogas (CH_4 and CO_2) is measured by displacing of liquid. In order to determine CH_4 concentration, every 5h a gas sample is sent to a gaseous phase chromatograph.

The input COD is selected by the operator when the bacteria are adapted to continuous operating conditions. The biomass adaptation to each different COD level requires 10 or 15 days. This is verified via the pH and methane flow rate variations, which become constant when the biomass is adapted. For purposes of this test, the COD is varied each day.

The substrate time evolution is detected measuring the COD, which is an indicator of the pollution in the substrate. The measure of this variable is easy, but it requires at least 3 h and has to be done off-line. COD is usually measured in anaerobic wastewater treatment plants and it is associated with S_2 concentration.

At the beginning of continuous experiment, when the acidogenesis phase begins the pH decreases, and if its value becomes less than 6, the process can be biologically destabilized due to acidification. To avoid this situation, it is advisable to keep pH close to 7.The biogas composition is an indicator of the biological activity inside the reactor. The substrate can be considered as totally transformed when the biogas production becomes negligible; then the biological reaction is over.

3.3.2   Experimental results

Data of pH measurement, COD measurements and biogas production measurement are used to calculate the model states (1)-(8) described in chapter 2. Input substrate S_{2in} is considered as proportional to the input substrate COD and output substrate COD is considered as proportional to the S_2. The outputs of the system are the Y_{CH_4} and Y_{CO_2} flows, defined by equations (6) and (7) described in chapter 2, respectively. From previous experiments [70], the Y_{CH_4} constitutes around 70% of the produced biogas and the Y_{CO_2} remaining is around 30%. Experimental results are compared with the values obtained from the observer as shown Figure 16Figure 16. The observer parameters S_{1in}, S_{2in} and $X_{2,0}$ for this test are decrement a 50 %.
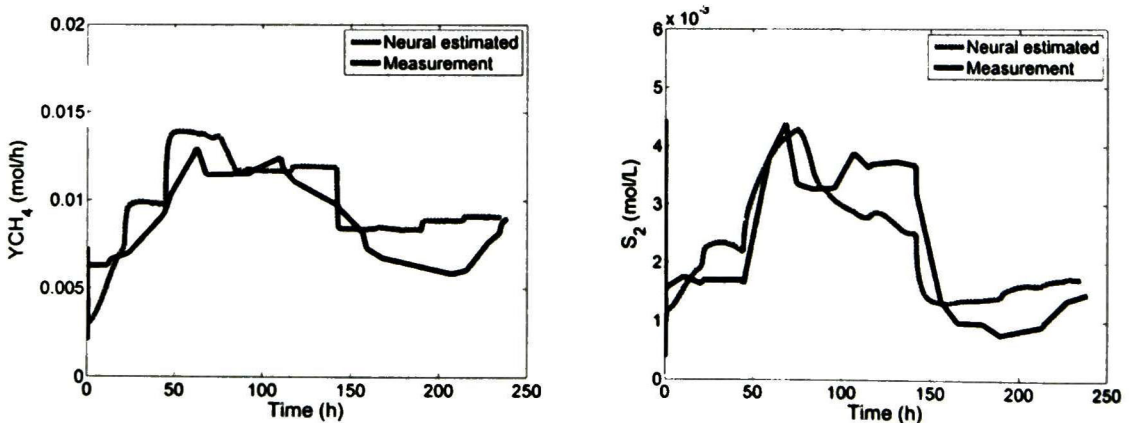
Figure 16 Observer and measurements comparison

Figure 16 illustrates a good estimation with a transient state error for Y_{CH_4} and S_2. This transient error may be due to the input substrate changes due to disturbances or could be due to the observer structure, which is a simple one. Additionally, in the model, X_2 is considered fixed on the solid support (zeolite) and does not contain the effect of the inputs; this affects the observer since the only way of access to X_2 is through the output (biogas). Despite this, estimation convergence speed from observer presents a good performance.

Since the biomass cannot be measured, X_2 is calculated using the model (validated experimentally in [13]) and the on-line pH measures. Model is compared with the values obtained from the observer. Figure 17 display such comparison.
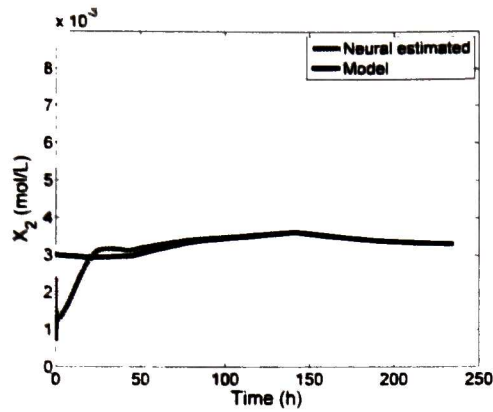
Figure 17 Biomass estimation

As can be seen, X_2 is estimated with a negligible transient error; this error could be induced by the abrupt change on the input substrate; anyway the estimation converges and the error is eliminated in steady state. Despite the errors in transient state, the RHONO is able to estimate adequately X_2 and S_2 of methanogenesis stage. Thus, it can be noticed that the proposed neural observer is a good alternative to estimate the important states of the anaerobic process.

Chapter 4

Control strategy synthesis and validation

This chapter discusses hybrid intelligent control, speed-gradient inverse optimal neural control, TS fuzzy supervisors for reference trajectories, gain scheduling and selection of controllers. The proposed neuronal observer is integrated into the hybrid intelligent control scheme, which keeps the process operating in presence of disturbances. A PSO optimization algorithm is implemented in order to improve the trajectory tracking.

4.1 Control scheme

In this section, a hybrid intelligent control structure is presented in order to control the methane production in presence of disturbances; this control strategy allows to choose an appropriate control action as a function of the system operating conditions. Reference trajectories for different states are calculated by a TS fuzzy supervisor in order to obtain a desired methane production.

4.1.1 Inverse optimal control strategy

Speed-gradient inverse optimal neural controllers for trajectory tracking are developed on the basis of the above mentioned neural observer. Two controllers are designed: a **base supplying ($b_{inc,k}$) action to regulate CO_2-bicarbonate equilibrium** and a **dilution rate ($D_{in,k}$) action to reject large disturbances in the input substrate**, respectively. A fuzzy supervisor is implemented in order to apply speed-gradient inverse optimal neural control actions. Fuzzy reference trajectories for the system states and Y_{CH_4} are implemented in order to force the system to track them. The process works in open loop in presence of small disturbances and for large disturbances, inverse optimal control actions are applied avoiding washout.

RHONO as an affine system. The proposed RHONO (62) is formulated as an affine system (25) with the aim of a speed-gradient inverse optimal control design for the AD system. Equation (87) corresponds to function f and (88) to function g. Equation (89) illustrates f, g and $x_{\delta,k+1}$ (reference trajectories) in vector form.

$$f_1\left(\hat{X}_{2,k}, \hat{IC}_k\right) = w_{11}S\left(\hat{X}_{2,k}\right) + w_{12}S^2\left(\hat{X}_{2,k}\right) + w_{13}S\left(\hat{IC}_k\right) + g_1 e_k,$$

$$f_2\left(\hat{S}_{2,k}, \hat{IC}_k\right) = w_{21}S\left(\hat{S}_{2,k}\right) + w_{22}S^2\left(\hat{S}_{2,k}\right) + w_{23}S\left(\hat{IC}_k\right)$$

$$+ w_{25}S^2\left(\hat{S}_{2,k}\right)S_{2in,k} + g_2 e_k,$$

$$f_3\left(\hat{X}_{2,k}, \hat{IC}_k\right) = w_{31}S\left(\hat{IC}_k\right) + w_{32}S^2\left(\hat{IC}_k\right) + w_{33}S\left(\hat{X}_{2,k}\right) + g_3 e_k \tag{87}$$

$$G_{11}(\hat{X}_{2,k}) = w_{14}S^2\left(\hat{X}_{2,k}\right) \qquad G_{12}(\hat{X}_{2,k}) = w_{14}S^2\left(\hat{X}_{2,k}\right)$$

$$G_{21}(\hat{S}_{2,k}) = w_{24}S^2\left(\hat{S}_{2,k}\right) \qquad G_{22}(\hat{S}_{2,k}) = 0 \tag{88}$$

$$G_{31}(\hat{IC}_k) = w_{34}S^2\left(\hat{IC}_k\right) \qquad G_{32}(\hat{IC}_k) = w_{35}S^2\left(\hat{IC}_k\right)$$

$$g_1(x_k) = \begin{bmatrix} G_{11} \\ G_{21} \\ G_{31} \end{bmatrix} \qquad g_2(x_k) = \begin{bmatrix} G_{12} \\ G_{22} \\ G_{32} \end{bmatrix}$$

$$f(x_k) = \begin{bmatrix} f_1 \\ f_2 \\ f_3 \end{bmatrix} \qquad x_{\delta,k} = \begin{bmatrix} X_{2ref,k} \\ S_{2ref,k} \\ IC_{ref,k} \end{bmatrix} \tag{89}$$

According to (52), the inverse optimal control law is formulated as

$$D_{in,k} = -\frac{1}{2}\left(R_{C1}(z_k) + \frac{1}{2}g_1^T(x_k)P_{g1}g_1(x_k)\right)^{-1}g_1^T(x_k)P_{g1}\left(f(x_k) - x_{\delta,k}\right) \tag{90}$$

$$b_{inc,k} = -\frac{1}{2}\left(R_{C2}(z_k) + \frac{1}{2}g_2^T(x_k)P_{g2}g_2(x_k)\right)^{-1}g_2^T(x_k)P_{g2}\left(f(x_k) - x_{\delta,k}\right) \tag{91}$$

where the positive definite matrix $P_{gi} = p_{ki} P_{Ci}$ is calculated by the SG algorithm, $R_{Ci}(z_k)$ is a constant matrix, $g_i(x_k)$ and $f(x_k)$ are matrices as in (89), for $i = 1,2$. Parameter values for inverse optimal control are in Table 5, appendix A.

The tracking of a desired trajectory, defined in terms of the plant state $x_{i,k}$ formulated as (58) can be established as the following inequality:

$$\left\| x_{i,\delta,k} - x_{i,k} \right\| \leq \left\| x_{i,k} - \hat{x}_{i,k} \right\| + \left\| x_{i,\delta,k} - \hat{x}_{i,k} \right\| \tag{92}$$

where $\|.\|$ stands for the Euclidean norm, $\hat{x}_{i,k}$ is the observed state, $x_{i,\delta,k}$ is the desired trajectory signal, which is assumed smooth and bounded. Inequality (92) is valid considering the separation principle for discrete-time nonlinear systems [30], and based on (92), the tracking of a desired trajectory can be divided into the following two requirements:

Requirement 1:

$$\lim_{t \to \infty} \left\| x_{i,k} - \hat{x}_{i,k} \right\| \leq \zeta_i \tag{93}$$

with ζ_i a small positive constant.

Requirement 2:

$$\lim_{t \to \infty} \left\| x_{i,\delta,k} - \hat{x}_{i,k} \right\| = 0. \tag{94}$$

An on-line neural observer trained with EKF based on (9) ensures (93) [71], while (94) is guaranteed by a discrete controller developed using inverse optimal control law.

4.1.2   Fuzzy supervisor structure

The AD process works in open loop in presence of small disturbances. However, for large disturbances, anaerobic microorganisms can die, and methane production stopped. Therefore, in order to solve this situation, a TS fuzzy supervisor [72], [73] for controllers selection is implemented. This supervisor allows a smooth switching between open loop and closed loop, avoiding washout. In order to force the system to produce methane at different disturbance magnitudes, a TS supervisor is designed to calculate reference trajectories for the system states and methane production. Finally, a TS supervisor for fuzzy gain scheduling is implemented in order to calculate gains for the controllers at different operating points. The applicability of the proposed scheme is illustrated via simulations.

4.1.2.1   *Fuzzy supervisor for controllers*
The supervisor has two main tasks: i) detect the process state, and ii) select the most adequate control action allowing smooth switching (if required) between them. The idea is to detect the attraction region

where the process is working; if any operating conditions cause the process to move away from the operating domain, the supervisor must determine and apply the control action which allows the bacteria to grow in order to avoid washout. Besides, if a variation on the operating conditions can be managed by the process itself, the supervisor must allow the system to operate in open loop, which represents energy saving. These objectives are achieved monitoring the variables that are indicators of the biological activity inside the reactor as a consequence of variations on the operating conditions. Organic daily load per biomass unit (ODL/X_2) variable is proposed for the fuzzy inference rules. ODL/X_2 represents the maximal quantity of organic load that a biomass unit can treat during a working day.

Each process stage has different reaction rates according to the substrate composition, and the stable development of the global process will require a balance that avoids the accumulation of inhibitors intermediate compounds or the accumulation of volatile fatty acids (VFA), which decrease the pH. Substrate pH must be kept close to neutrality. The CO_2-bicarbonate equilibrium is important for the pH stability. On the other hand, large input substrate disturbances which cannot be treated by the biomass require to be rejected. Therefore, a first control action in closed loop is required to regulate acidification and a second to reject large disturbances and avoid washout. There exists a limit of ODL/X_2 to which the process can operate in open loop, after that require a control action. Then, the input disturbances can be classified by this variable into small, average and large. For this reason, three fuzzy sets are determined as shown in Figure 18.
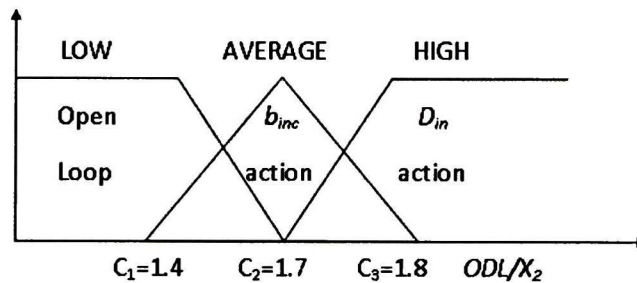
Figure 18 *ODL/X₂* fuzzyfication

The ODL/X_2 is defined as:

$$ODL / X_2 = D_{in} A_2 S_{20} / \hat{X}_2, \tag{95}$$

where D_{in} is the dilution rate (h^{-1}), A_2 a disturbance amplitude on the substrate input S_{2in} (mol L^{-1}), S_{20} the initial value of the substrate S_2 (mol L^{-1}) and $\hat{X}_2$ is the estimated biomass X_2 (mol L^{-1}).

Concerning the output fuzzy variables, three operation regions for the process are identified as function of the ODL/X_2: open loop which represents energy saving, closed loop with b_{inc} action which contributes to CO_2-bicarbonate equilibrium and closed loop with D_{in} action to reject large disturbances. The number of fuzzy sets is determined from simulations in order to classify the input variables behavior as a function of the operation conditions. Then, three fuzzy inference rules are deduced (96)-(98):

$$\text{If } ODL \, / \, X_2 \text{ is LOW then } u_1 = \text{open loop} \tag{96}$$

$$\text{If } ODL \, / \, X_2 \text{ is AVERAGE then } u_2 = b_{inc,k} \text{ action} \tag{97}$$

$$\text{If } ODL \, / \, X_2 \text{ is HIGH then } u_3 = D_{in,k} \text{ action} \tag{98}$$

Defuzzification is done using the average center method [72]:

$$u = \frac{\sum_{j=1}^{R} \gamma_j u_j}{\sum_{j=1}^{R} \gamma_j} \tag{99}$$

with R the number of rules, γ_j is known as the membership function and is calculated as $\gamma_j = \gamma_{ODL/X_2}^k$

where γ_{ODL/X_2}^k is the membership degree of variable ODL/X_2 on the fuzzy set, k the k^{st} fuzzy set of ODL/X_2

and $\sum_{j=1}^{R} \gamma_j = 1.$

In presence of a disturbance on S_{2in}, ODL/X_2 can abruptly increase up to a value, which exceeds the conditions of stability limits (critical value); therefore the process tends to washout or system instability. If ODL/X_2 is above its critical value then a control law must be applied in order to allow biomass growth, and hence, diminishing ODL/X_2 and stabilizing the system. In contrast, if the ODL/X_2 is under its critical value then the system can work in open loop. Depending on the ODL/X_2 value, commutation between operating modes (open loop, closed loop) is done by a TS fuzzy supervisor. This commutation takes place progressively in order to avoid abrupt switching. The main idea of this control scheme is to combine different control actions in order to minimize their drawbacks and to profit from their advantages. Consequently, the most adequate control action is applied in order to avoid washout. The structure of the hybrid intelligent control is shown in the Figure 19.
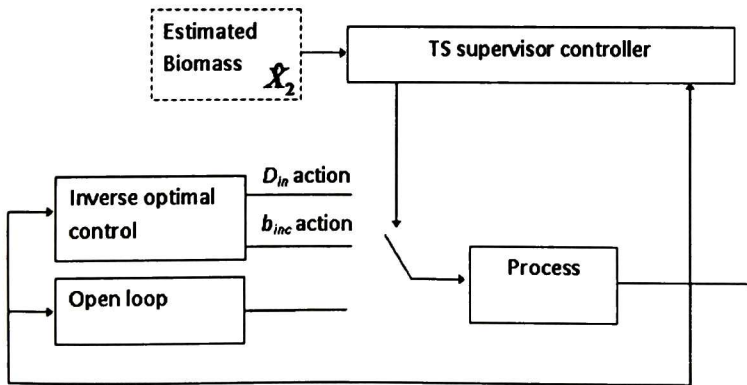

Figure 19 TS supervisor for controllers

4.1.2.2 Fuzzy supervisor of reference trajectories

The inverse optimal neural control algorithm requires reference trajectories to force the system to track them. The proposed reference trajectories are taken from a previous work [65], because they represent an optimal dynamic behavior of the anaerobic process for growth biomass and methane production in presence of disturbances. Five trajectories from low to high disturbances on input substrate are calculated. In order to obtain global reference trajectories, a TS supervisor for is implemented. The specific structure is based on five trajectories, which are interpolated by a fuzzy algorithm in order to obtain the global reference trajectories in presence of disturbances. The inference rules are composed of linguistic variables as premises and varying-time reference trajectories (instead of linguistic variables) as consequents [74]. For the premises, the input disturbance S_{2in} is selected as the fuzzy input variable and 5 fuzzy sets are proposed, as illustrated in Figure 20.
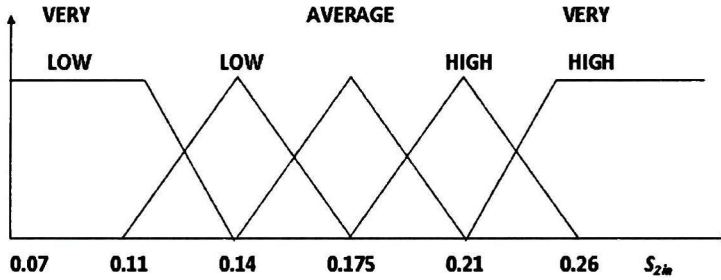
Figure 20 S_{2in} **fuzzyfication**

Each fuzzy set corresponds to a different disturbance amplitudes; for each amplitude, a reference trajectory is synthesized. From the fuzzy variable and the different reference trajectories, five inference rules are deduced as follows:

$$\text{If } S_{2in} \text{ is VERY LOW then } x_{ref} = xr_1, \ y = C_1 x_{ref} \tag{100}$$

$$\text{If } S_{2in} \text{ is LOW then } x_{ref} = xr_2, \ y = C_2 x_{ref} \tag{101}$$

$$\text{If } S_{2in} \text{ is AVERAGE then } x_{ref} = xr_3, \ y = C_3 x_{ref} \tag{102}$$

$$\text{If } S_{2in} \text{ is HIGH then } x_{ref} = xr_4, \ y = C_4 x_{ref} \tag{103}$$

$$\text{If } S_{2in} \text{ is VERY HIGH then } x_{ref} = xr_5, \ y = C_5 x_{ref} \tag{104}$$

$x_{ref} = x_{\delta,k}$ corresponds to reference trajectories for X_2, S_2 and IC. From this fuzzy rules structure, it is easy to see that the active reference trajectories at each instant are determined by S_{2in}. The global reference trajectory is calculated using the defuzzyfication algorithm [74] described by:

$$x_{ref} = \frac{\sum_{j=1}^{R} \gamma_j \{xr_j\}}{\sum_{j=1}^{R} \gamma_j} \tag{105}$$

$$YCH_{4ref} = \frac{\sum_{j=1}^{R} \gamma_j \{C_j x_{ref}\}}{\sum_{j=1}^{R} \gamma_j} \tag{106}$$

where γ_j is the membership function and determined as $\gamma_j = \gamma_{S_{2in}}^k$ whit $\gamma_{S_{2in}}^k$ the membership degree of variable S_{2in} on the respective fuzzy set.

The scheme of the reference trajectories supervisor is shown on the Figure 21.
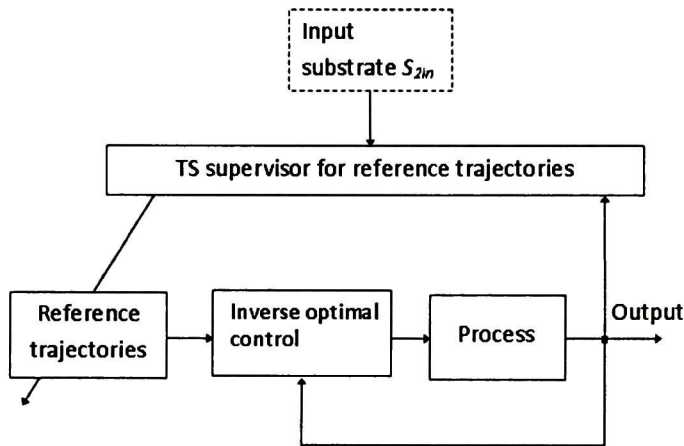
Figure 21 TS supervisor for reference trajectories

4.1.2.3 Fuzzy supervisor gain scheduling

With global reference trajectories the control algorithm requires to tune the gains of the controllers. In order to simplify this tuning task, a fuzzy gain scheduling is implemented [74]. For the rules, the input disturbance S_{2in} is selected as the input variable because control actions tuning depends of disturbance amplitude. A TS supervisor detects the disturbance amplitude on the input substrate and implements a fuzzy interpolation to keep updating the gain of the controller. Fuzzy sets are the same as illustrated in Figure 20.

For each one of the disturbance amplitude, an inverse optimal neural control (90)-(91) is synthesized in order to regulate the substrate around an operating point. The corresponding gains of the nonlinear controllers are determined according to the inverse optimal control approach and are used as output variables in the consequents. Hence, the fuzzy rules have the structure:

$$\text{If } S_{2in} \text{ is VERY LOW then } K_f = K_{D1} \tag{107}$$

$$\text{If } S_{2in} \text{ is LOW then } K_f = K_{D2} \tag{108}$$

$$\text{If } S_{2in} \text{ is AVERAGE then } K_f = K_{D3} \tag{109}$$

$$\text{If } S_{2in} \text{ is HIGH then } K_f = K_{D4} \tag{110}$$

$$\text{If } S_{2in} \text{ is VERY HIGH then } K_f = K_{D5} \tag{111}$$

Gain K_D is applied in the inverse optimal control law as follows:

$$D_{in,k} = -\frac{K_D}{2}\left(R_{C1}(z_k) + \frac{1}{2}g_1^T(x_k)P_{g1}g_1(x_k) \right)^{-1} g_1^T(x_k)P_{g1}\left(f(x_k) - x_{\delta,k+1} \right). \tag{112}$$

Time-varying gain K_B for $b_{inc,k}$ control is calculated on a similar way.
The global gain is calculated using the defuzzyfication equation described by:

$$K_f = \frac{\sum_{j=1}^{R} \gamma_j \{K_{Dj}\}}{\sum_{j=1}^{R} \gamma_j} \tag{113}$$

where γ_j is the membership function and determined as $\gamma_j = \gamma_{S_{2in}}^k$ whit $\gamma_{S_{2in}}^k$ the membership degree of variable S_{2in} on the respective fuzzy set. The scheme is shown in Figure 22.
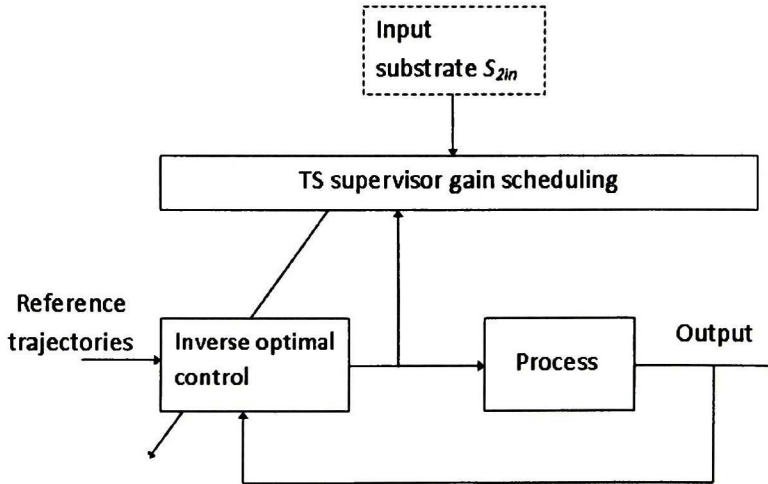
Figure 22 TS supervisor for gain scheduling

The whole hybrid intelligent control scheme is displayed in Figure 23.
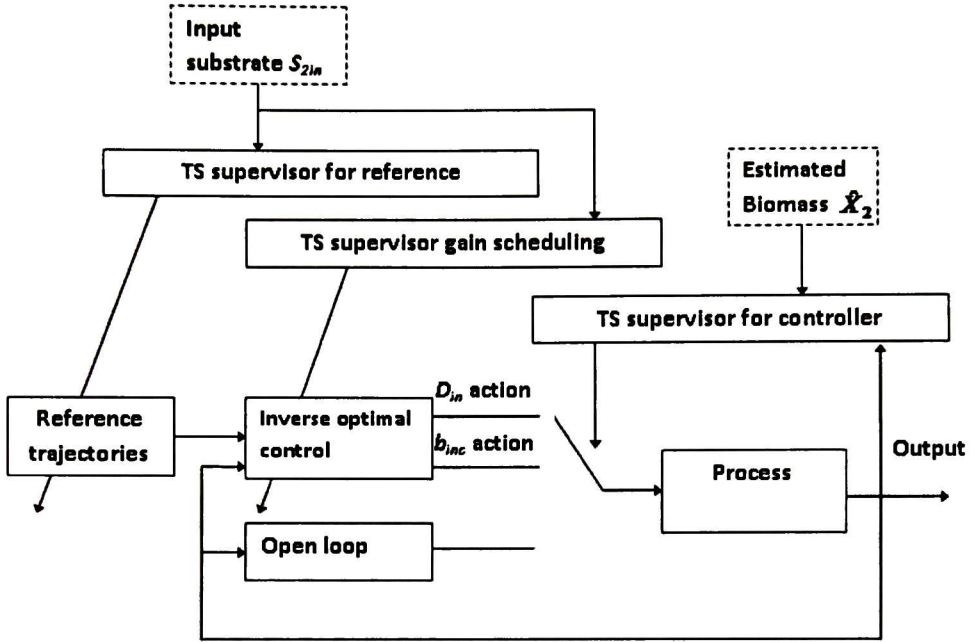
Figure 23 Integrated hybrid intelligent control scheme

Integrated hybrid intelligent control scheme improves the performances of the anaerobic process and is feasible for application in real processes, since the control scheme shows a good compromise between efficiency and complexity.

The convergence analysis of this control scheme is stated as the following theorem.

Theorem 3: Consider that the neural system (62) in affine form (87)-(88) with control law (43) has achieved the SG control goal (45) by means of (49). Then, the inverse optimal control law with fuzzy reference trajectory (100)-(104) and time-varying gain (107)-(111) renders solution $\hat{x}_k$ of system (62) to be globally asymptotically stable along the desired trajectory $x_{\delta,k}$. Moreover, inverse optimal control law (52) minimizes the cost functional (53).

Proof. Let $V_{sg}\left(z_{q,k}\right) = \frac{1}{2}z_{q,k}^T P_C z_{q,k}$ be a Lyapunov function candidate with $P_C = P_C^T > 0$ and $z_{q,k} = x_{\delta,k} - \hat{x}_k$. Considering that system (62) in affine system form, with control law (43) and (49) has achieved the SG control goal (45) for $k \geq k^*$, then (45) can be rewritten as

$$V_{sg}\left(z_{q,k+1}\right)-V_{sg}\left(z_{q,k}\right)+\frac{1}{\bar{p}}u_k^{*T}R\left(z_{q,k}\right)u_k^{*}=$$

$$\frac{1}{2}z_{q,k+1}^{T}P_C z_{q,k+1}-\frac{1}{2}z_{q,k}^{T}P_C z_{q,k}+\frac{1}{\bar{p}}u_k^{*T}R\left(z_{q,k}\right)u_k^{*}\leq 0 \tag{114}$$

with

$$u_k^{'}=-\frac{K_u}{2}\left(R\left(z_{q,k}\right)+\frac{1}{2}g^{T}\left(x_k\right)P_g g\left(x_k\right)\right)^{-1}g^{T}\left(x_k\right)P_g\left(f\left(x_k\right)-x_{ref}\right). \tag{115}$$

where K_u represents K_D and K_B time-varying gains for $u_{k\_D in,k}$ and $u_{k\_b inc,k}$ controllers respectively, x_{ref} corresponds to global reference trajectories and $P_g = \bar{p}\, P_C$.

Thus, multiplying (114) by the positive constant $\bar{p}$, we obtain

$$\begin{aligned}\bar{V} &= \frac{\bar{p}}{2}z_{q,k+1}^{T}P_C z_{q,k+1}-\frac{\bar{p}}{2}z_{q,k}^{T}P_C z_{q,k}+u_k^{*T}R\left(z_{q,k}\right)u_k^{*}\\ &=\frac{1}{2}z_{q,k+1}^{T}P_g z_{q,k+1}-\frac{1}{2}z_{q,k}^{T}P_g z_{q,k}+u_k^{*T}R\left(z_{q,k}\right)u_k^{*}\\ &=V\left(z_{q,k+1}\right)-V\left(z_{q,k}\right)+u_k^{*T}R\left(z_{q,k}\right)u_k^{*}\leq 0\end{aligned} \tag{116}$$

and condition (38) is fulfilled. From (116), $V\left(z_{q,k+1}\right)-V\left(z_{q,k}\right)\leq 0$ is satisfied for all $z_{q,k}\neq 0$ and therefore global asymptotic stability is achieved in accordance with Theorem 1. When function $-l(x_k)$ is set to be the (116) right-hand side, then:

$$l\left(z_{q,k}\right)=-\left(V\left(z_{q,k+1}\right)-V\left(z_{q,k}\right)\right)+\alpha^{T}\left(z_{q,k}\right)R\left(z_{q,k}\right)\alpha\left(z_{q,k}\right)>0 \tag{117}$$

$\forall z_{q,k}\neq 0$, minimize the cost functional:

$$J=\sum_{k=0}^{\infty}\left(l\left(z_{q,k}\right)+u_k^{T}R\left(z_{q,k}\right)u_k\right) \tag{118}$$

In order to obtain the optimal value function for the cost functional (118), we substitute (117) into (118) to obtain:

$$\begin{aligned}J &= \sum_{k=0}^{\infty}\left(l\left(z_{q,k}\right)+u_k^{T}R\left(z_{q,k}\right)u_k\right)\\ &=-\sum_{k=0}^{\infty}\left(V\left(z_{q,k+1}\right)-V\left(z_{q,k}\right)\right)+\sum_{k=0}^{\infty}\left(u_k^{T}R\left(z_{q,k}\right)u_k-\alpha^{T}\left(z_{q,k}\right)R\left(z_{q,k}\right)\alpha\left(z_{q,k}\right)\right).\end{aligned} \tag{119}$$

with

$$\alpha\left(z_{q,k}\right) := u_k^*$$
$$= -\frac{1}{2}\left(R\left(z_{q,k}\right) + \frac{1}{2}g^T\left(x_k\right)P_k g\left(x_k\right)\right)^{-1} g^T\left(x_k\right)P_k\left(f\left(x_k\right) - x_{\delta,k+1}\right) \tag{120}$$

the optimal control law. After evaluating (119) for $k = 0$, then it can be written as

$$J = -\sum_{k=1}^{\infty}\left(V\left(z_{q,k+1}\right) - V\left(z_{q,k}\right)\right) - V\left(z_{q,1}\right) + V\left(z_{q,0}\right)$$
$$+ \sum_{k=0}^{\infty}\left(u_k^T R\left(z_{q,k}\right)u_k - \alpha^T\left(z_{q,k}\right)R\left(z_{q,k}\right)\alpha\left(z_{q,k}\right)\right)$$
$$= -\sum_{k=2}^{\infty}\left(V\left(z_{q,k+1}\right) - V\left(z_{q,k}\right)\right) - V\left(z_{q,2}\right) + V\left(z_{q,1}\right) - V\left(z_{q,1}\right) + V\left(z_{q,0}\right) \tag{121}$$
$$+ \sum_{k=0}^{\infty}\left(u_k^T R\left(z_{q,k}\right)u_k - \alpha^T\left(z_{q,k}\right)R\left(z_{q,k}\right)\alpha\left(z_{q,k}\right)\right).$$

For notation convenience in (121), the upper limit ∞ will be considered as $N \to \infty$, and therefore

$$J = -V\left(z_{q,N}\right) + V\left(z_{q,N-1}\right) - V\left(z_{q,N-1}\right) + V\left(z_{q,0}\right)$$
$$+ \sum_{k=0}^{N}\left(u_k^T R\left(z_{q,k}\right)u_k - \alpha^T\left(z_{q,k}\right)R\left(z_{q,k}\right)\alpha\left(z_{q,k}\right)\right) \tag{122}$$
$$= -V\left(z_{q,N}\right) + V\left(z_{q,0}\right) + \sum_{k=0}^{N}\left(u_k^T R\left(z_{q,k}\right)u_k - \alpha^T\left(z_{q,k}\right)R\left(z_{q,k}\right)\alpha\left(z_{q,k}\right)\right).$$

Letting $N \to \infty$ and noting that $V(z_{q,N}) \to 0$ for all $z_{q,0}$, then

$$J\left(z_{q,k}\right) = V\left(z_{q,0}\right) + \sum_{k=0}^{\infty}\left(u_k^T R\left(z_{q,k}\right)u_k - \alpha^T\left(z_{q,k}\right)R\left(z_{q,k}\right)\alpha\left(z_{q,k}\right)\right). \tag{123}$$

Thus, the minimum value of (123) is reached with $u_k = \alpha(z_{q,k})$. Hence, the control law (120) minimizes the cost functional (118). The optimal value function of (118) is $J^*(z_{q,N}, \alpha(z_{q,k})) = V(z_{q,0})$ for all $z_{q,0}$. $\square$

4.2 Control scheme validation

A set of simulations close to experimental conditions **are presented** to validate the proposed control strategy. The presented results correspond to the experiment with the largest experimentation time. The

control scheme **is tested** in presence of disturbances on the input substrate and parameter variations on the growth rate. Initial conditions for η_D and observer states are the same as the third test of the previous chapter.

First, the proposed strategy is tested in presence of a 120 % disturbance on S_{2in}, incepted at t=200 hours. Trajectories tracking for states and Y_{CH_4} are illustrated in Figure 24.
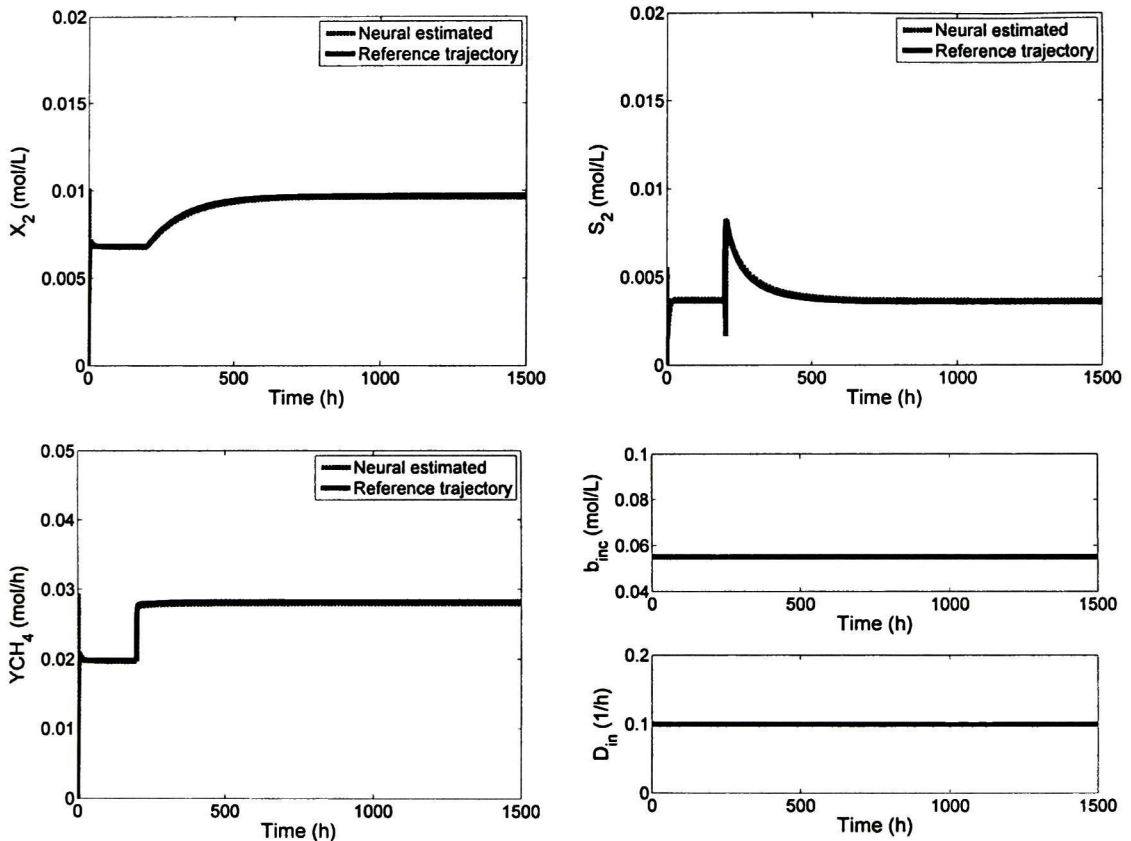
Figure 24 Trajectories tracking states for a 120 % disturbance

When the disturbance is introduced on the input substrate, the fuzzy supervisors determine adequate reference trajectories and control law in order to allow biomass growth, diminishing ODL/X_2 and stabilizing the system. As can be seen, the process operates in open loop because the disturbance is small; this is due to the fact that ODL/X_2 belongs to the associated fuzzy set corresponding to open loop (Figure 18). This situation implies that the AD process is able to work adequately without control ($b_{inc,k}$ and $D_{in,k}$ have the respective equilibrium value) in presence of this small disturbance. Thus, the response of the system is stable during all process time. The Y_{CH_4} is calculated with equation (65), which is based on the observed system states.

A second test for the integrated hybrid control strategy is done introducing a 165 % disturbance on S_{2in} incepted at t=200 hours, as illustrated in Figure 25.

Figure 25 Trajectories tracking states for a 165 % disturbance

For this disturbance, integrated hybrid intelligent control strategy operates in closed loop because the disturbance is large and a control action is required. During disturbance, ODL/X_2 increases its value until reaching a level corresponding to HIGH fuzzy set (Figure 18). Therefore, the system goes to closed loop operation mode applying control action $D_{in,k}$. During the evolution process ODL/X_2 diminishes its level and starts to belong to HALF fuzzy set. Thus, control action $b_{inc,k}$ is applied and the control action $D_{in,k}$ is stopped. Finally, ODL/X_2 diminishes its value until belonging to the fuzzy set associated to open loop. This situation implies that the disturbance has been rejected completely. Under these last conditions, supervisor stops the action $b_{inc,k}$ and the process returns to its operation in open loop. Thus, trajectory references for the states and Y_{CH_4} are reached with error approaching zero on the steady state as illustrated in Figure 25. This error could be due to which the control law requires a better tuning.

A third test for the proposed integrated hybrid intelligent control strategy is introducing a 200 % disturbance on S_{2in} incepted at t=200 hours, as is illustrated in Figure 26.
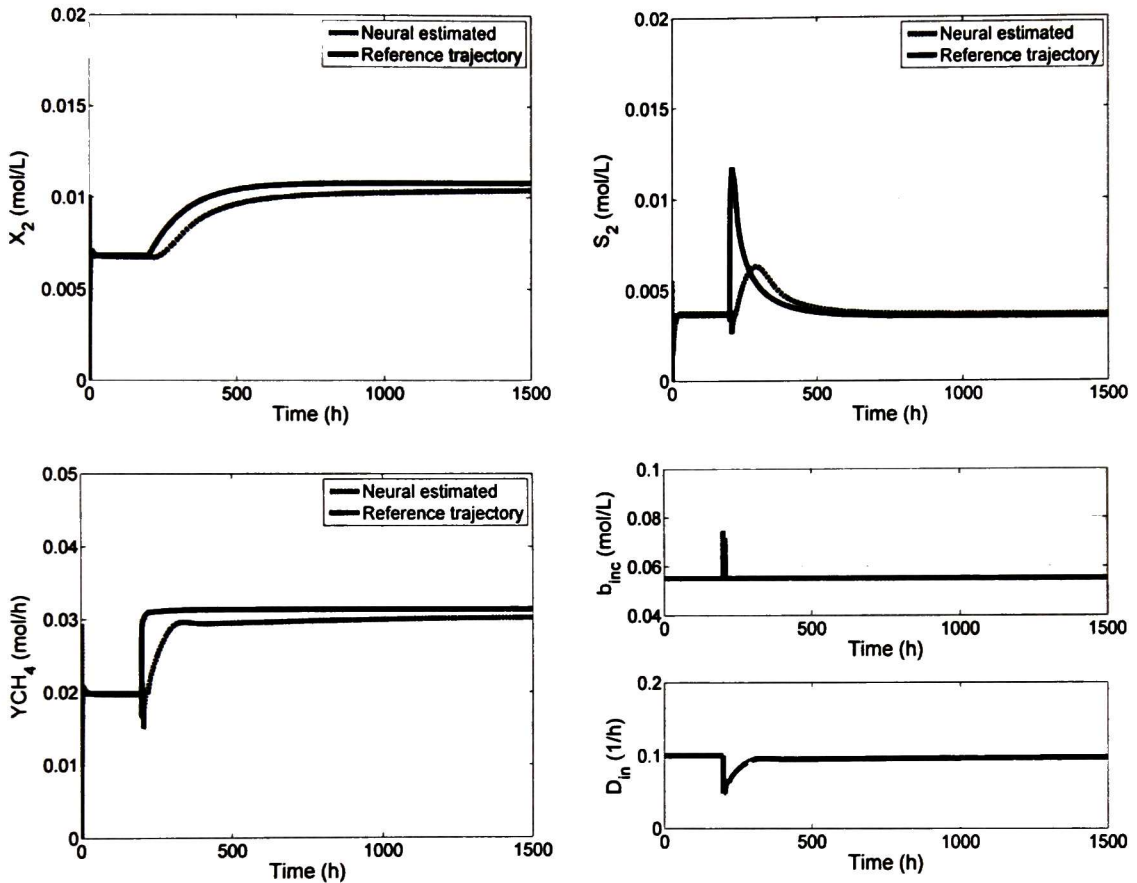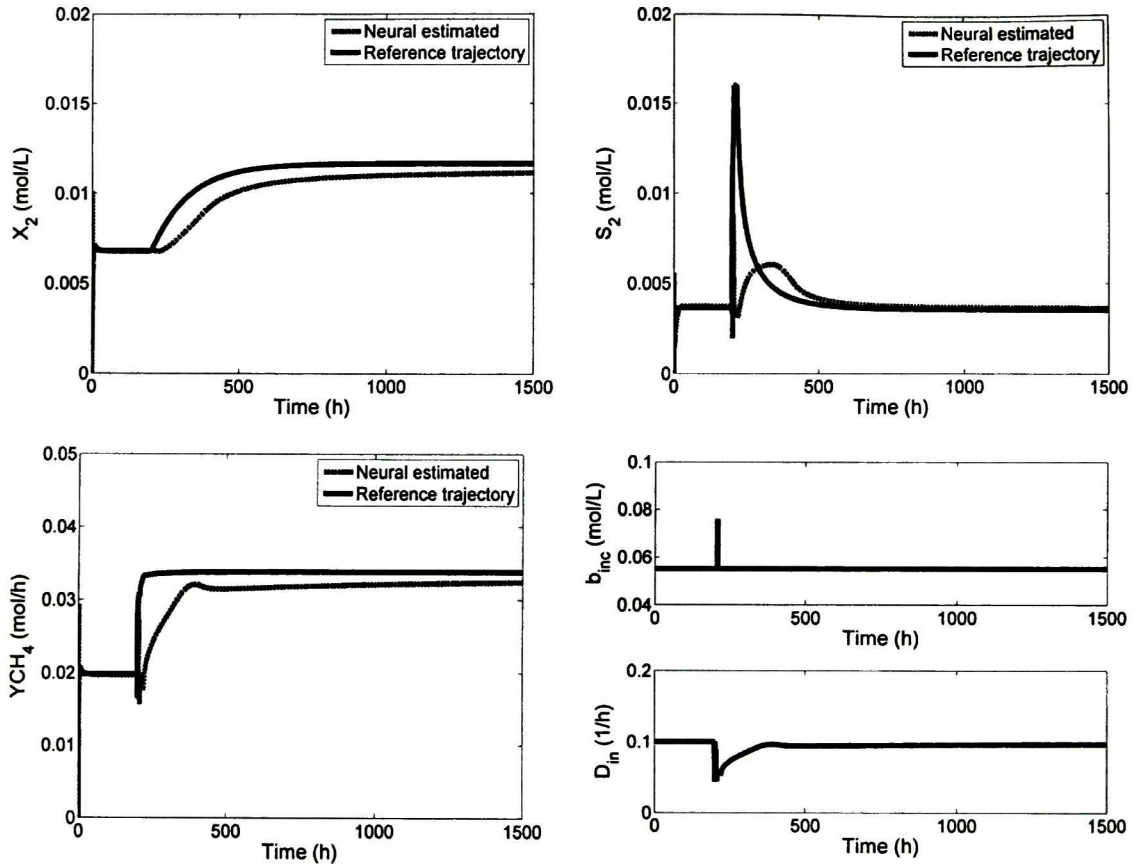

Figure 26 Trajectories tracking for a 200 % disturbance

As can be seen, the control strategy detects a large disturbance and the fuzzy supervisors determine adequate reference trajectories and control action to be applied until the disturbance is rejected. Thus, reference trajectories for the states and Y_{CH_4} are reached and the error approaches zero on the steady state as illustrated in Figure 26. As in the previous test, this error could be eliminated with an optimal tuning of the control law. Corresponding $b_{inc,k}$ and $D_{in,k}$ control signals are displayed. System operation is ensured because control strategy is applied, even though a large disturbance is incepted.

Finally, control strategy tolerance to change in the system parameters is tested; such variation is incepted as a disturbance on the bacteria concentration, μ_{1max} and μ_{2max} as presented in Table 3, appendix A, and a disturbance on the input substrate of 200 % S_{2in} increase incepted at t=200 h as in Figure 26. Performance of the system is illustrated in Figure 27.
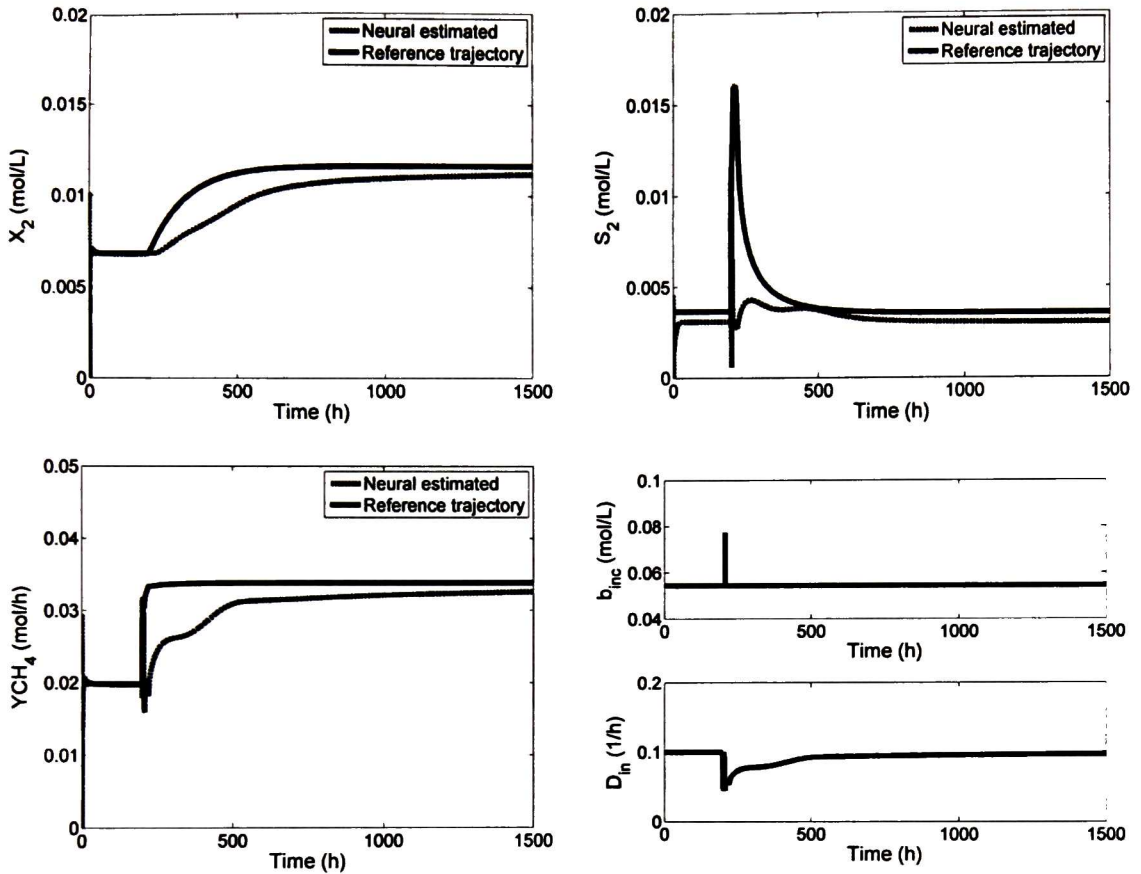
Figure 27 Trajectories tracking for parameter variation

As it is illustrated in Figure 27, AD system presents a transient state error due to disturbance in rate growth parameters which affect directly the kinetic; the control strategy acts in order to reject the disturbances and to track the trajectory which is achieved on steady state with a small error. Reference trajectories are achieved and the robustness of the proposed RHONO to parameters variations is verified. Thus, the proposed control strategy is efficient in order to control the AD process.

For the case of disturbances larger than 200 % on S_{2in}, the oscillation induced by the observer **prevents** the supervisor to control the process. Therefore, the system tends to washout. Thus, a critical value exists for which the supervisor cannot control the bio-process due to the magnitude of the disturbances.

4.3   Particle swarm optimization

PSO is a population-based algorithm, which exploits a population of potential solutions to probe the search space concurrently. The population is called the *swarm* and its individuals are called the *particles*; a

notation retained by nomenclature used for similar models in social sciences and particle physics [75]. PSO is based on simulation models of social behavior; thus, an information exchange mechanism shall exist to allow particles to mutually communicate their experience. The algorithm approximates the global minimizer with the best position ever visited by all particles. Therefore, it is a reasonable choice to share this crucial information.

4.3.1 Algorithm description

For the PSO algorithm, each member of the population is treated as a point in a D-dimensional space [76]. Let, $A \subset R^n$, be the search space, and, $f : A \rightarrow Y \subset R$, be the objective function. In order to keep descriptions as simple as possible, we assume that A is also the feasible space of the problem at hand, i.e., there are no further explicit constraints posed on the candidate solutions. The swarm is defined as a set:

$$S = \left\{ x_{1d}, x_{2d}, ..., x_{Nd} \right\} \tag{124}$$

of N particles (candidate solutions), defined as:

$$x_{id} = \left(x_{i1}, x_{i2}, ..., x_{in} \right)^T \in A, \quad i = 1, 2, ..., N. \tag{125}$$

Indices are arbitrarily assigned to particles, while N is a user-defined parameter of the algorithm. The objective function, $f(x)$, is assumed to be available for all points in A. Thus, each particle has a unique function value, $fi = f(x_i) \in Y$.

The particles are assumed to move within the search space, A, iteratively. This is possible by adjusting their *position* using a proper position shift, called *velocity*, and denoted as:

$$v_{id} = \left(v_{i1}, v_{i2}, ..., v_{in} \right)^T \quad i = 1, 2, ..., N. \tag{126}$$

Velocity is updated based on information obtained in previous steps of the algorithm. This is implemented in terms of a memory, where each particle can store the *best position* it has ever visited during its search. For this purpose, besides the swarm, S, which contains the current positions of the particles, PSO maintains also a *memory* set:

$$P = \left(p_{1d}, p_{2d}, ..., p_{Nd} \right), \tag{127}$$

which contains the best positions:

$$p_{id} = \left(p_{i1}, p_{i2}, ..., p_{in} \right)^T \in A, \quad i = 1, 2, ..., N, \tag{128}$$

ever visited by each particle. These positions are defined as:

$$P_{id,k} = \arg\min_{k} f_{i,k},$$

(129)

where k stands for the iteration counter.

The best particle among all the particles (the global best position) is represented by p_{gd}. Let gd be the index of the best position with the lowest function value in P at a given iteration k, i.e.,

$$P_{gd,k} = \arg\min_{i} f\left(p_{id,k}\right).$$

(130)

Then, the early version of PSO is defined by the following equations [76]:

$$v_{id} = v_{id} + c_1 rand_1 \left(p_{id} - x_{id}\right) + c_2 rand_2 \left(p_{gd} - x_{id}\right)$$

(131)

$$x_{id} = x_{id} + v_{id}$$

(132)

where c_1 and c_2 are weighting factors, also called the *cognitive* and *social* parameter, respectively. $rand_1$ and $rand_2$ are random variables uniformly distributed within [0, 1]. The performance of each particle is measured according to a predefined fitness function, which is related to the problem to be solved [75].

At each iteration, after the update and evaluation of particles, best positions (memory) are also updated. Thus, the new best position of x_{id} at iteration $k+1$ is defined as follows:

$$P_{id,k+1} = \begin{cases} x_{i,k+1}, & \text{if } f\left(x_{i,k+1}\right) \leq f\left(p_{i,k}\right), \\ p_{i,k}, & otherwise. \end{cases}$$

The new determination of index gd for the updated best positions completes an iteration of PSO. Particles are usually initialized randomly, following a uniform distribution over the search space, A. This choice treats each region of A equivalently; therefore it is mostly preferable in cases where there is no information on the form of the search space or the objective function, requiring a different initialization scheme. The previous velocity term, $v_{id,k}$, in the right-hand side of equation (131), offers a means of inertial movement to the particle by taking its previous position shift into consideration. This property can prevent it from becoming biased towards the involved best positions, which could entrap it to local minima if suboptimal information is carried by both (e.g., if they both lie in the vicinity of a local minimizer).

Furthermore, the previous velocity term serves as a perturbation for the global best particle, x_{gd}. Indeed, if a particle, x_i, discovers a new position with lower function value than the best one, then it becomes the global best (i.e., $gd \leftarrow i$) and its best position, p_{id}, will coincide with p_{gd} and x_{id} in the next iteration. Thus, the two stochastic terms in equation (131) will vanish. If there was no previous velocity term in equation (131), then the aforementioned particle would stay at the same position for several iterations, until a new best position is detected by another particle. Contrary to this, the velocity term allows this particle to continue its search, following its previous position shift.

The values of c_1 and c_2 can affect the search ability of PSO by biasing the sampled new positions of a particle, x_i, towards the best positions, p_{id} and p_{gd}, respectively, as well as by changing the magnitude of search. If a better global exploration is required, then high values of c_1 and c_2 can provide new points in relatively distant regions of the search space. On the other hand, a more refined local search around the best positions achieved so far would require the selection of smaller values for the two parameters. Also, choosing, $c_1 > c_2$, would bias sampling towards the direction of p_{id}, while in the opposite case, $c_1 < c_2$, sampling towards the direction of p_{gd} would be favored. This effect can be useful in cases where there is special information regarding the form of the objective function. For instance, in convex unimodal objective functions, a choice that promotes sampling closer to p_{gd} is expected to be more efficient, if combined with a proper search magnitude. For more detail of PSO algorithm see reference [75].

4.3.2 PSO application to the AD process

In this dissertation, the PSO algorithm is employed to find the P_C matrix elements for SG inverse optimal control. Figure 28 shows a block diagram which illustrates how PSO algorithm affects the AD process control scheme, by means of the matrices P_{C1} and P_{C2} of the $u_{k\_D_{in,k}}$ and $u_{k\_b_{inc,k}}$ actions, respectively. The algorithm computes the matrices which minimize the mean square tracking error between the estimated biomass $\hat{x}_{2,k}$ and its given trajectory reference $x_{\delta,k}$.
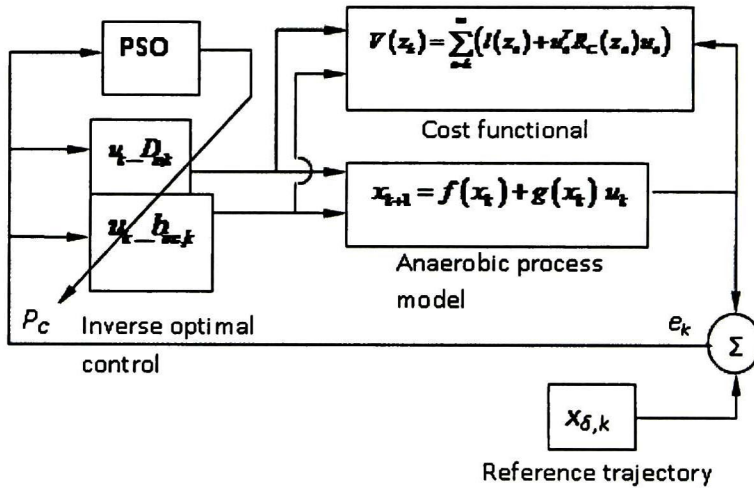
Figure 28 PSO Hybrid intelligent inverse optimal control Scheme

4.3.3 PSO algorithm validation for the AD process

Test 1. The proposed control strategy is tested introducing a large disturbance of 150% on S_{2in}, incepted at t=200 hours. Matrices P_{C1} and P_{C2} (133) for $u_{k\_D_{in,k}}$ and $u_{k\_b_{inc,k}}$ respectively, are selected heuristically such that the system (62) to be asymptotically stable along the desired trajectory $x_{\delta,k}$. The selected matrices are

$$P_{C1} = \begin{bmatrix} 23300 & 1112 & 2028 \\ 1112 & 422 & 310 \\ 2028 & 310 & 354 \end{bmatrix} \quad P_{C2} = \begin{bmatrix} 355 & 164 & 160 \\ 164 & 669 & 492 \\ 160 & 492 & 583 \end{bmatrix} \quad (133)$$

Trajectories tracking for $X_{2,k}$ and Y_{CH_4} are illustrated in Figure 29, where the continuous line is the reference trajectory signal and the dotted line is the system output signal.
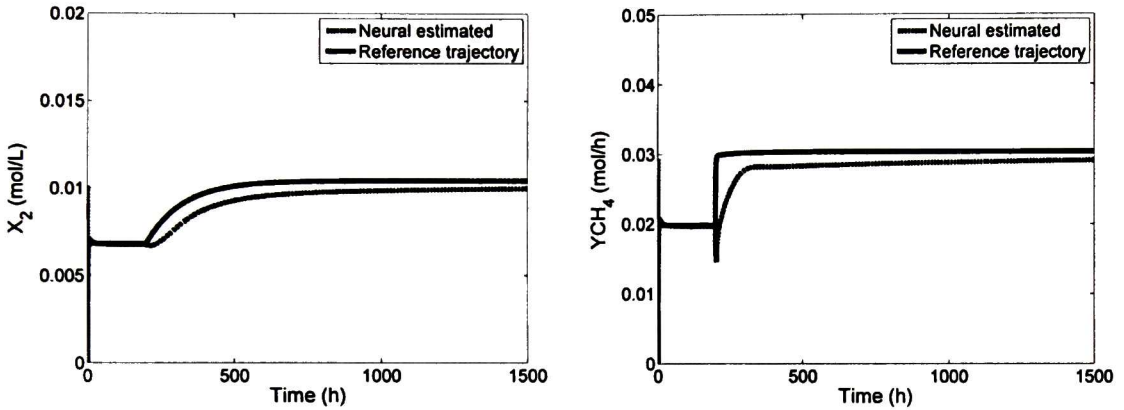
Figure 29 Trajectory tracking for a 150 % disturbance

As can be seen, with this disturbance, the trajectory references for $X_{2,k}$ and Y_{CH_4} are reached with a transient error which approaching zero on the steady state.

Test 2. PSO algorithm is used in order to find the matrices P_{C1} and P_{C2} for the control laws. PSO algorithm parameters used for this control scheme are shown in Table 6 from appendix A. With these parameters, the output matrices of the PSO algorithm are:

$$P_{C1} = \begin{bmatrix} 58530 & 918 & 3463 \\ 918 & 914 & 869 \\ 3463 & 869 & 1033 \end{bmatrix} \quad P_{C2} = \begin{bmatrix} 820.65 & 1017.78 & 444.23 \\ 1017.78 & 1386.91 & 520.29 \\ 444.23 & 520.29 & 335.70 \end{bmatrix} \quad (134)$$

Simulation with the new matrices is done for the same conditions as in the previous test; the results are illustrated in Figure 3030.

Figure 30 PSO Trajectory tracking for a 150 % disturbance

In Table 7 (Appendix A), a mean square error (MSE) comparison between test 1 and test 2 is displayed. For test 2, reference trajectory is achieved at minor time with a smaller transient error as shown in Table 7. Hence, the proposed control law based on PSO algorithm shows a better performance. In order to test this control scheme with different reference trajectories, the system is disturbed introducing a large disturbance of 200 % on S_{2in}, incepted at t=200 hours.

Test 3. First, matrices P_{C1} and P_{C2} heuristically determined in (133) are selected. Figure 311 illustrates trajectories tracking for $X_{2,k}$ and Y_{CH_4}
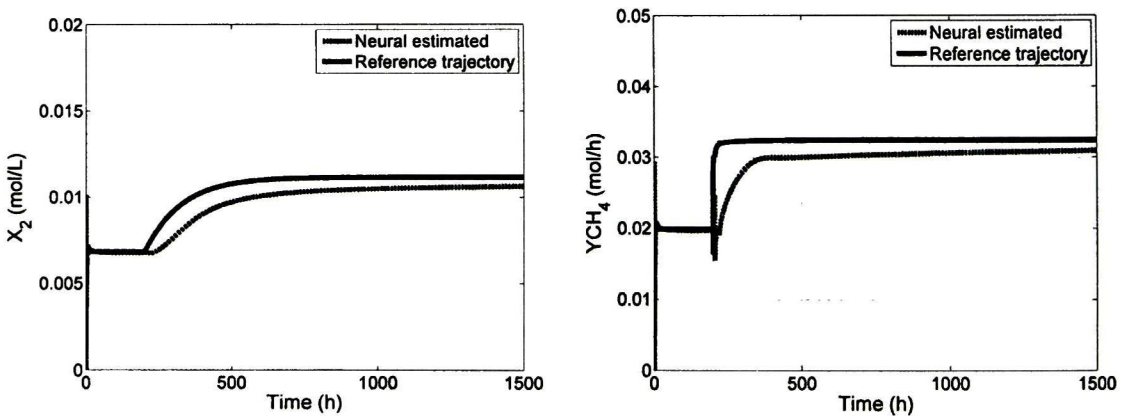
Figure 31 Trajectory tracking for a 200 % disturbance

This test illustrates a big error in transient state which approaching zero on the steady state. Trajectory references for $X_{2,k}$ and Y_{CH_4} are never reached with this matrices.

Test 4. In this test, matrices P_{C1} and P_{C2} calculated with a PSO algorithm are selected (134) . Figure 32 illustrates trajectories tracking for $X_{2,k}$ and Y_{CH_4}
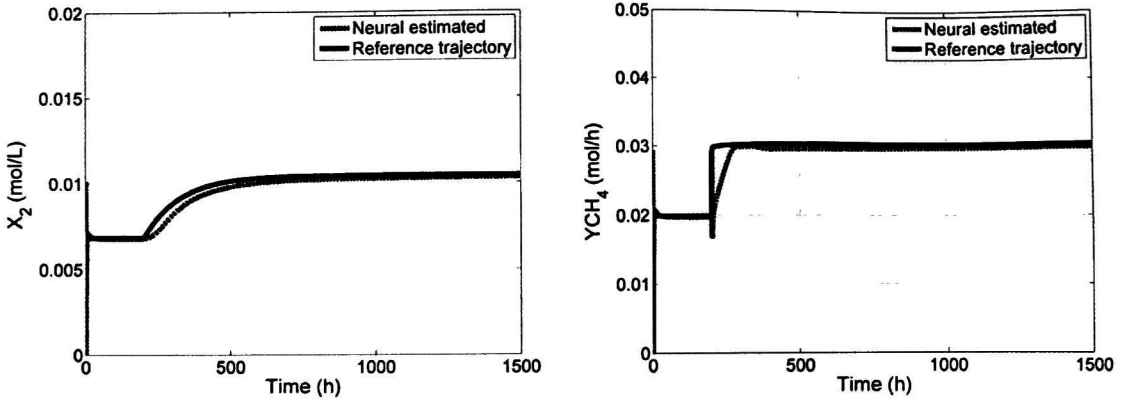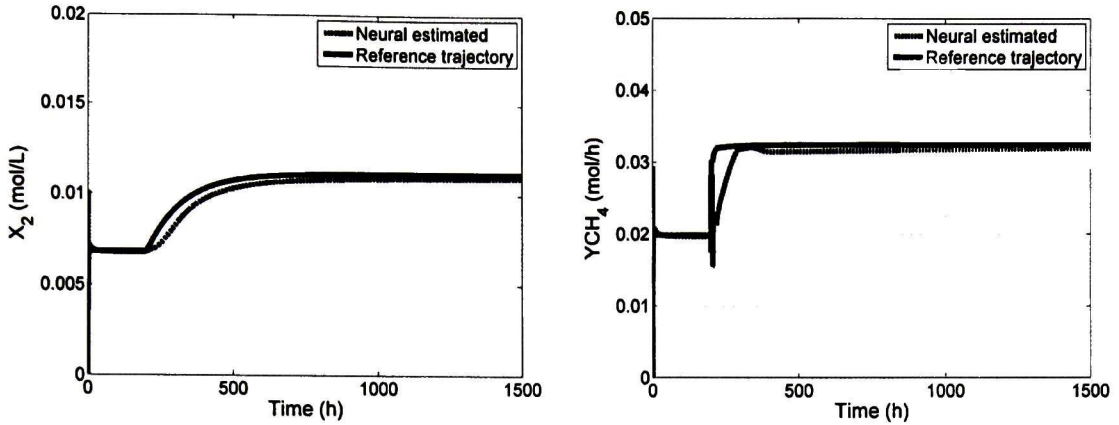
Figure 32 PSO Trajectory tracking for a 200 % disturbance

On Table 8 (appendix A), a MSE comparison between test 3 and test 4 is presented. As can be seen, for this test trajectory tracking is achieved with a smaller MSE in transient state. Hence, the proposed control law based on PSO algorithm is the best in order to reach reference trajectories. PSO algorithm is a good strategy in order to calculate matrix elements of inverse optimal control because diminishing the tracking error and the system reaches the reference in minor time. Figure 33 displays PSO algorithm evolution MSE for $X_{2,k}$ with initial value MSE = $0.2.54 \times 10^{-5}$ and final value MSE = 1.7×10^{-7}.
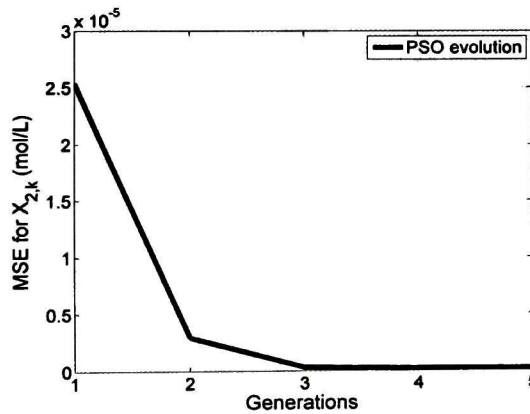
Figure 33 PSO evolution

For AD process control law, PSO algorithm calculates five generations with $rand_1$ and $rand_2$ selected as random 4-dimensional vectors with their components uniformly distributed within [0,1]. Figure 33 illustrates the minimization of the MSE for estimated $X_{2,k}$ at each iteration. It is concluded that the PSO algorithm calculates P_C matrix optimal parameters which enhanced the convergence speed of the system to the reference trajectory and the error in the steady state is eliminated.

Chapter 5

Conclusions and future work

5.1 Conclusions

In this dissertation, an integrated hybrid intelligent control strategy scheme for an anaerobic wastewater treatment process is proposed. The main objective is a continuous methane production in presence of disturbances and to avoid washout. In order to reach this, biological, physicochemical and hydrodynamic behaviors of anaerobic process is modeled. This model is composed by a fast stage for acetate production and methanogenesis stage for methane production considered as the limiting stage. This process is developed in a CSTR with biomass filter in continuous mode. With the purpose of satisfied the main objective, a nonlinear discrete-time recurrent high order neural observer (RHONO) trained with an EKF is used to estimate the biomass concentration, substrate concentration, and inorganic carbon from the methanogenesis stage. These variables are estimated from CH_4 and CO_2 flow rates, which are commonly measured in this process. In addition, is assumed that pH and the process inputs are on-line measured. One of the principal contributions of this dissertation is a methodology to obtain a time-varying learning rate (η_D), in order to enhance the performance of neuronal observers. η_D is proposed as a function of the pH substrate because is a determining variable in the process operation. Simulation results illustrate the observer effectiveness with η_D in presence of disturbances and parameter variation. Thus, observer robustness is proven and is a good alternative to estimate important states of AD process.

With the purpose of achieves the second objective of this dissertation, an experimental validation for the observer is performed in order to verify its performance in presence of disturbances. The experiment is performed in a prototype bioreactor of 7 L in continuous mode during ten days. In this test, the next variables are measured: pH, biogas, input substrate COD and output substrate COD. The input substrate COD is varied each day with the purpose of verifies the performance in presence of disturbances. Experimental validation of the observer illustrates that it is a good alternative to estimate on-line important states and Y_{CH_4} of the AD process. Since one of the limiting factors in the implementation of control

strategies is the lack of on-line sensors, the results of this neuronal observer are an alternative adequate that can be applied in continuous bioreactors for wastewater treatment.

On the other hand, once this neural observer is obtained, it can be integrated to control strategies. Fuzzy supervisors and speed-gradient inverse optimal control law, based on this neural observer, are developed and they form the Hybrid intelligent inverse optimal control. Thus, a third objective of this dissertation is satisfied. Two speed-gradient inverse optimal neural controllers for trajectory tracking are developed: a base supplying ($b_{inc,k}$) action to regulate CO_2-bicarbonate equilibrium and a dilution rate ($D_{in,k}$) action to reject large disturbances in the input substrate, respectively. The process works in open loop in presence of small disturbances which represents energy saving.

A fourth objective of this work is the implementation of TS supervisors to be integrated into the control scheme. First a TS supervisor for controllers is implemented. It detects biological activity inside the tank reactor, on the basis of estimated biomass, and selects between open and closed loop actions depending on the disturbance amplitude. A second TS supervisor for reference trajectory generates reference trajectories for the system states and Y_{CH_4}, on the basis of the disturbance amplitude on the input substrate. Finally, a third TS supervisor gain scheduling detects the disturbance amplitude on the input substrate and interpolates adequate gains for the controllers. The goal is to force the system to track desired reference trajectories avoiding washout. Simulation results show that the integrated hybrid intelligent control scheme is able to stabilize the methane production along of desired trajectories in presence of disturbances and parameter variations. Trajectory references are reached with error approaching zero on the steady state. This error could be due to the fact that the control law requires a better tuning. However, control action fulfills the objectives of rejecting disturbances, and obtaining a high efficiency of the process, which is reflected in a good production of biogas. With this achievement, a fifth objective of this dissertation is achieved.

As a last objective, a PSO algorithm for parameter optimization is employed to find the P_C matrix elements for SG inverse optimal control. In previous tests P_C matrix is selected heuristically such that the system to be asymptotically stable along the desired trajectory $x_{\delta,k}$. However results illustrate a steady state error which approaches zero. In order to solve this problem PSO algorithm is implemented. Results with this approach illustrated which the PSO algorithm calculates P_C matrix optimal parameters which enhanced the convergence speed of the system to the reference trajectory and the error in the steady state is eliminated.

5.2   Future work

As future work, it is worth to mention:

The exosystem for reference trajectories may be obtained from laboratory experiments.

Experimental validation of the neural observer can be enhanced by performing more experiments in continuous mode.

Reset adaptive observer for nonlinear systems could be implemented for AD process.

Covariance matrices P_i, Q_i and R_i of EKF for NN learning, may be calculated with PSO algorithm.

Implementation in real-time of the proposed RHONO and the control scheme for an AD process.

Bibliography

[1]. R. H., Williams, E. D., Larson, R. E., Katofsky and J., Chen, Methanol and Hydrogen from Biomass for Transportation, *Energy for Sustainable Development: The Journal of the International Energy Initiative*, 1(5), 18-34, 1995.

[2]. C. N., Hamelinck and A. P.C. Faaij, Future prospects for production of methanol and hydrogen from biomass, *Journal of Power Sources*, 111, 1-22, 2002.

[3]. L. R., Clausen, N., Houbak and B., Elmegaard, Technoeconomic analysis of a methanol plant based on gasification of biomass and electrolysis of water, *Energy*, 35(5), 2338-2347, 2010.

[4]. S., Carlos-Hernandez, G., Mallet and J. F., Beteau, Modeling and analysis of the anaerobic digestion process, *Proceedings of IFAC Symposium on Structures Systems and Control*, Oaxaca, Mexico, 2004.

[5]. S. A., Smith and C. O., Stöckle, A biogas meter with adjustable resolution and minimal back-pressure, *Bioresource Technology*, 99, 8537-8539, 2008.

[6]. R. O., Cadena Pereda, E. M., Rivera Muñoz and G., Herrera Ruiz, Automatic volumetric gas flow meter for monitoring biogas production from laboratory-scale anaerobic digester, *Sensors and Actuators B: Chemical*, 147(1), 10-14, 2010.

[7]. A., Rodriguez, G., Quiroz, J., de Leon, and R., Femat, State and parameter estimation of an anaerobic digester model, *Automation Science and Engineering (CASE), 2011 IEEE Conference on*, 690 – 695, 2011.

[8]. D., Paesa, A., Baños and C., Sagues, Optimal reset adaptive observer design, *Systems & Control Letters*, 60(10), 877-883, 2011.

[9]. D., Paesa, C., Franco, S., Llorente, G., Lopez-Nicolas and C. Sagues, Reset observers applied to MIMO systems, *Journal of Process Control*, 21(4), 613-619, 2011.

[10]. V., Alcaraz-Gonzalez, and V., Gonzalez- Alvarez, Robust nonlinear observers for Bioprocesses: Application to wastewater treatment (Book Chapter in Selected Topics in Dynamics and Control of Chemical and Biological Processes), Springer-Verlag, pp 119–164, Berlin, Germany, 2007.

[11]. M., Moisan, O., Bernard and J-L., Gouzé, Near optimal interval observers bundle for uncertain bioreactors, *Automatica*, 45(1), 291-295, 2009.

[12]. D. A., Urrego-Patarroyo, E. N., Sanchez, S., Carlos-Hernandez and J. F., Beteau, Recurrent neural networks biomass observer for anaerobic processes, *IEEE Multi-Conference on Systems and Control*, San Antonio, Texas, USA, 2008.

[13]. R., Belmonte-Izquierdo, S., Carlos-Hernández and E. N., Sánchez, A new neural observer for an anaerobic bioreactor, *International Journal of Neural Systems*, 20(1), 75–86, 2010.

[14]. S., Haykin, *Neural Networks: A comprehensive Foundation*, 2nd Ed., Prentice Hall, New Jersey, USA, 1999.

[15]. A. S., Poznyak E.N., Sanchez and W., Yu, *Differential Neural Networks for Robust Nonlinear Control*, World Scientific Publishing Co., Singapore, 2001.

[16]. G.A., Rovithakis and M.A., Chistodoulou, *Adaptive Control with Recurrent High-Order Neural Networks*, Springer Verlag, Berlin, Germany, 2000.

[17]. M., Madsen, J. B., Holm-Nielsen and K. H., Esbensen, Monitoring of anaerobic digestion processes: A review perspective, *Renewable and Sustainable Energy Reviews*, 15(6), 3141-3155, 2011.

[18]. M. R., Kosseva and C.A., Kent, *Modeling, Monitoring, and Process Control for Intelligent Bioprocessing of Food Industry Wastes and Wastewater Chapter 11*, Food Industry Wastes, 191-213, 2013.

[19]. K., Jiayu, W., Mengxiao, X., Zhongjun and Z., Yan, Fuzzy PID Control of the PH in an Anaerobic Wastewater Treatment Process, *Intelligent Systems and Applications*, 1-4, 2009.

[20]. J., Batstone and J. P., Steyer, Use of modelling to evaluate best control practice for winery-type wastewaters. *Water Science and Technology*, 52(2), 147-152, 2007.

[21]. J. P., Garcia-Sandoval, V., Gonzalez-Alvarez, B., Castillo-Toledo and C., Pelayo-Ortiz, Robust discrete control of nonlinear processes: application to chemical reactors, *Computer Chemical Engineering*, 32(12), 3246-3253, 2008.

[22]. S. Stoyanov, Robust multiple-input-multiple-output control of non-linear continuous fermentation processes, *Bioprocess and Biosystems Engineering*, 23(4), 309-314, 2000.

[23]. E., Petre, D., Selisteanu and D., Sendrescu, Adaptive control strategies for a class of anaerobic depollution bioprocesses, *Proceedings of IEEE International Conference on Automation, Quality and Testing, Robotics*, Cluj-Napoca, Romania, 2008.

[24]. N., Hilgert, J., Harmand, J-P., Steyer and J-P., Vila, Nonparametric identification and adaptive control of an anaerobic fluidized bed digester, *Control Engineering Practice*, 8(4), 367-376, 2000.

[25]. J., Seok, Hybrid adaptive optimal control of anaerobic fluidized bed bioreactor for the de-icing waste treatment, *Journal of Biotechnology*, 102(2), 165-175, 2003.

[26]. A. Rincón, C. Erazo and F. Angulo, A robust adaptive controller for an anaerobic digester with saturated input: Guarantees for the boundedness and convergence properties, *Journal of Process Control*, 22(9), 1785-1792, 2012.

[27]. C., Waewsak, A., Nopharatana, and P. Chaiprasert, Neural-fuzzy control system application for monitoring process response and control of anaerobic hybrid reactor in wastewater treatment and biogas production, *Journal of Environmental Sciences*, 22(12), 1883-1890 2010.

[28]. A., Ordace, C. M., Ionescu, T.P.W., Vannecke, I.P.E., Volcke, I., Nascu and R., De Keyser, Predictive control of anaerobic digestion of wastewater sludge. A feasibility study , *System Theory, Control and Computing (ICSTCC), 2012 16th International Conference on*, 1 – 7, 2012.

[29]. M. Francisco, P. Vega and S. Revollar, Model predictive control of BSM1 benchmark of wastewater treatment process: a tuning procedure, 50th IEEE CDC-ECC, Orlando, Florida, USA, 7057-7062, 2011.

[30]. F., Ornelas, E. N., Sanchez and A. G., Loukianov, Discrete-time inverse optimal control for nonlinear systems trajectory tracking, *Proceedings of the 49th IEEE Conference on Decision and Control*, Atlanta, Georgia, USA, 2010.

[31]. F., Ornelas, E. N., Sanchez, A. G., Loukianov and E. M. Navarro-Lopez, Speed-Gradient Inverse Optimal control for Discrete-Time Nonlinear Systems, *Proceedings of 50th IEEE Conference on Decision and Control and European Control Conference*, Orlando, Florida, USA, 2011.

[32]. B. S., Leon, A. Y., Alanis, E. N., Sanchez, F., Ornelas and E., Ruiz-Velazquez, Inverse optimal trajectory tracking for discrete time nonlinear positive systems, *Proceedings of 50th IEEE Conference on Decision and Control and European Control Conference*, Orlando, Florida, 2011.

[33]. F., Monnet, *An Introduction to Anaerobic Digestion of Organic Wastes*, Final Report by Remade Scotland Initiative, Paris, France, 2003.

P. L., McCarty, Anaerobic waste treatment fundamentals, *Public Works*, 95(9), 107-112, 1964.

[34]. A. L., Fradkov and A. Y., Pogromsky, *Introduction to Control of Oscillations and Chaos*, World Scientific Publishing Co, Singapore, 1998.

[35]. A., Rozzi, Modelling and control of anaerobic digestion process, *Transactions Instrumentation, Modelling and Control*, 6(3), 153-159, 1984.

[36]. P. T., Williams, *Waste Treatment & Disposal 2nd Edition*, John Wiley & Sons, London, UK.

[37]. Y., Chen, J. J., Cheng and K. S., Creamer, Inhibition of anaerobic digestion process: a review. *Bioresource Technology*, 99(10), 4044–4064, 2007.

[38]. V., Otton, Axial dispersion of liquid in fluidized bed with external recycling: two dynamic modeling approaches with a view to control, *Biochemical Engineering Journal*, 4 (2) 129–136, 2000.

[39]. J. F., Beteau, *An industrial wastewater treatment bioprocess modelling and control*, PhD dissertation, INPG, Paris, France, 1992.

[40]. J. J., Heijnen and B., Romein, Derivation of kinetic equations for growth on single substrates based on general properties of a simple metabolic network, *Biotechnology. Prog.*, 11, 712-716, 1995.

[41]. R., Segers, Methane production and methane consumption: a review of processes underlying wetland methane fluxes, *Biogeochemistry*, 41, 23-51, 1998.

[42]. B., Zhang, S., Xu and Y., Zou, Relaxed stability conditions for delayed recurrent neural networks with polytopic uncertainties, *International Journal of Neural Systems* 16(6), 473–482, 2006.

[43]. B., Zhang, S., Xu and Y., Li, Delay-dependent robust exponential stability for uncertain recurrent neural networks with time-varying delays, *International Journal of Neural Systems* 17(3), 207–218, 2007.

[44]. G. G., Rigatos, Adaptive fuzzy control with output feedback for H∞ tracking of SISO nonlinear systems, *International Journal of Neural Systems*, 18(4), 305–320, 2008.

[45]. M., Gao, Robust exponential stability of markovian jumping neural networks with time-varying delay, *International Journal of Neural Systems* 18(3), 207–218, 2008.

[46]. M., Liu and S., Zhang, An LMI approach to design h∞ controllers for discrete-time nonlinear systems based on unified models, *International Journal of Neural Systems* 18(5), 443–452, 2008.

[47]. A.M.A., Haidar, A., Mohamed, M., Al-Dabbagh, A., Hussain, M.A.S. Masoum, An intelligent load shedding scheme using neural networks and neuro-fuzzy, *International Journal of Neural Systems*, 19(6), 473–479, 2009.

[48]. A. Y., Alanis, E. N., Sanchez, A. G., Loukianov and M. A., Perez, Real-time recurrent neural state estimation, *IEEE Transactions on, Neural Networks,* 22(3), 497–505, 2011.

[49]. W., Yu and X., Li, Nonlinear system identification using discrete-time recurrent neural networks with stable learning algorithms, *Information Sciences*, 158 131–147, 2004.

[50]. S. S., Ge, J., Zhang and T. H., Lee, Adaptive neural network control for a class of MIMO nonlinear systems with disturbances in discrete-time, *IEEE Transactions on Systems, Man and Cybernetics, Part B* 34(4), 2004.

[51]. E. N., Sanchez, A. Y., Alanis and G. R., Chen, Recurrent neural networks trained with the Kalman filtering for discrete chaos reconstruction, *Dyn. Continuous Discrete Impulsive Syst. B*, 13c, 1–18, 2007.

[52]. E. N., Sanchez, A. Y., Alanis and A. G., Loukianov, *Discrete Time High Order Neural Control Trained with Kalman Filtering*, Springer-Verlag, Berlin, Germany, 2008.

[53]. Y., Song and J. W., Grizzle, The extended Kalman filter as a local asymptotic observer for discrete-time nonlinear systems, *Journal of Mathematical Systems, Estimation and Control*, 5(1), 59–78, 1995.

[54]. S., Haykin, *Kalman Filtering and Neural Networks*, John Wiley and Sons, New York, USA, 2001.

[55]. D. E., Kirk, *Optimal Control Theory: An Introduction*, Prentice-Hall, New Jersey, USA, 1970.

[56]. T., Basar and G. J., Olsder, *Dynamic Noncooperative Game Theory*, 2nd Ed., Academic Press, New York, USA, 1995.

[57]. F. L., Lewis and V. L., Syrmos, *Optimal Control*, John Wiley and Sons, New York, USA, 1995.

[58]. A., Al-Tamimi and F. L., Lewis, Discrete-time nonlinear HJB solution using approximate dynamic programming: convergence proof, *IEEE Transactions on Systems, Man, Cybernetics-Part B*, 38(4), 943–949, 2008.

[59]. T., Ohsawa, A. M., Bloch and M., Leok, Discrete Hamilton-Jacobi theory, Retrieved July 12, 2011, from http://www.citebase.org/abstract?id=oai:arXiv.org:0911.2258, 2009.

[60]. W. M., Haddad, V.-S., Chellaboina, J. L., Fausz and C., Abdallah, Optimal discrete-time control for non-linear cascade systems, *Journal of The Franklin Institute*, 335(5), 827–839, 1998.

[61]. H. K., Khalil, *Nonlinear Systems*, Prentice Hall, Upper Saddle River, N. J., USA, 1996.

[62]. G. L., Amicucci, S., Monaco and D. Normand-Cyrot, Control Lyapunov stabilization of affine discrete-time systems, *Proceedings of the 36th IEEE Conference on Decision and Control*, San Diego, CA, pp. 923-924, 1997.

[63]. J. P., LaSalle, *The Stability and Control of Discrete Processes*. Springer-Verlag, New York, USA, 1986.

[64]. A. L. Fradkov and A. Y. Pogromsky, *Introduction to Control of Oscillations and Chaos* World Scientific, Singapore, 1998.

[65]. R., Belmonte-Izquierdo, S., Carlos-Hernandez and E. N., Sanchez, Hybrid Intelligent Control Scheme for an Anaerobic Wastewater Treatment Process, *Second International Workshop on Advanced Computational Intelligence* (IWACI 2009), Mexico City, Mexico, 2009.

[66]. Y. H., Kim and F. L., Lewis, *High-Level Feedback Control with Neural Networks*, World Scientific, Singapore, 1998.

[67]. L., Diaz-Jimenez, E., Herrera-Ramirez, and S., Carlos-Hernandez, Using natural zeolites to improve anaerobic abattoir wastewater treatment, *The Third International Meeting on Environmental Biotechnology and Engineering*, Palma de Mallorca, Spain, 2008.

[68]. R., Borja, E., Sanchez, P., Weiland, L., Travieso, and A., Martin, Kinetics of anaerobic digestion of cow manure with biomass immobilized on zeolite, *Chemical Engineering Journal*, 54(1), 1994.

[69]. J., Rodríguez, G. J., Sosa, and Y., Garza, Bioconversión anaerobia como una alternativa para la remoción de dqo contenido en aguas residuales del rastro municipal de la ciudad de Saltillo, Coahuila, México, *Journal of the Mexican Chemical Society*, 46(2), pp 185-188, 2002.

[70]. A., Bueno, Estructura híbrida de control para un proceso anaeróbico de tratamiento de efluentes, Tesis de maestría, Centro de Investigación y Estudios Avanzados del IPN, Guadalajara, México, 2012.

[71]. A. Y., Alanis, Discrete-time Neural Control: Application to Induction Motors, PhD thesis, Centro de Investigación y Estudios Avanzados del IPN, Guadalajara, México, 2007.

[72]. T., Takagi and M., Sugeno, Fuzzy identification of systems and its applications to modeling and control, *IEEE Trans. on Systems Man and Cybernetics*, 15(1), 116-132, 1985.

[73]. K. Passino and S. Yurkovich, *Fuzzy control*, NewYork: AddisonWesley Longman, Inc., 1998.

[74]. S., Carlos-Hernandez, N., Oudaak, J. F., Beteau and E. N., Sanchez, Fuzzy observer for the anaerobic digestion process, *Proceedings of IFAC Symposium on Structures Systems and Control*, Oaxaca, Mexico, 2004.

[75]. K. E., Parsopoulos and M. N., Vrahatis, *Particle Swarm Optimization and Intelligence*, Information Science Reference, New York, USA, pp. 25-40, 2010.

[76]. Y., Shi and R., Eberhar, A modified particle swarm optimizer, *IEEE Evolutionary Computation Proceedings,* Indianapolis, USA, pp. 69 – 73, 1998.

A. PARAMETER VALUES

Table 1. Parameter values for anaerobic digestion model

Kinetic parameters			Initial conditions		
Symbol	Value	Unit	Symbol	Value	Unit
μ_{1max}	0.205	h^{-1}	$X_{1,0}$	5.6836	mol L^{-1}
k_{s1}	0.26	mol L^{-1}	$S_{1,0}$	0.0537	mol L^{-1}
k_{i1}	16.333×10^{-4}	mol L^{-1}	$X_{2,0}$	0.0068	mol L^{-1}
μ_{2max}	0.017	h^{-1}	$S_{2,0}$	0.0037	mol L^{-1}
k_{s2}	2.18×10^{-5}	mol L^{-1}	IC_0	0.0817	mol L^{-1}
k_{i2}	8.22×10^{-3}	mol L^{-1}	Z_0	0.0551	mol L^{-1}
Equation parameters			D_{in}	0.1	h^{-1}
Symbol	Value	Unit	$S1_{in}$	10	mol L^{-1}
k_{d1}	0.035	h^{-1}	$S2_{in}$	0.07	mol L^{-1}
k_{d2}	0.0085	h^{-1}	IC_{in}	0.0051	mol L^{-1}
R_1	0.99		Z_{in}	0.0051	mol L^{-1}
R_2	0.99				
R_3	345				
R_4	0.0666				
R_5	0.0005				
R_6	5				
K_a	1.7×10^{-5}	mol L^{-1}			
K_b	1.7×10^{-7}	mol L^{-1}			
Kh	0.065	mol L^{-1} Pa^{-1}			
P_t	1	Pa			

Table 2. Parameter values for neural observer

Symbol	Value	Unit	Symbol	Value	Unit
$w_{11}, w_{12}, w_{13}, w_{14}, w_{15}$	0.0068	mol L^{-1}	g_{m1}	0.12	
$w_{21}, w_{22}, w_{23}, w_{24}, w_{25}$ w_{26}	0.0037	mol L^{-1}	g_{m2}	0.09	
$w_{31}, w_{32}, w_{33}, w_{34}, w_{35}$	0.0817	mol L^{-1}	g_{m3}	0.09	
$P_{1,0}$	1500		η_1	2	
$P_{2,0}$	1000		η_2	1	
$P_{3,0}$	1500		η_3	10	
$Q_{1,0}$	1.5		$\hat{X}_{2,1}$	0.0102	mol L^{-1}
$Q_{2,0}$	1.5		$\hat{S}_{2,1}$	0.0046	mol L^{-1}
$Q_{3,0}$	0.2		$\hat{IC}_1$	0.1223	mol L^{-1}
$R_{1,0}$	150				
$R_{2,0}$	150				
$R_{3,0}$	1.5				

Table 3. Parameter values variation

Symbol	Value	Unit
$\hat{X}_{2,1}$	0.0116	mol L^{-1}
$\hat{S}_{2,1}$	0.0052	mol L^{-1}
$\hat{IC}_1$	0.1386	mol L^{-1}
μ_{1max}	0.1845	h^{-1}
μ_{2max}	0.0188	h^{-1}

Table 4. Abattoir wastewater characteristics

Element	Value
Soluble solids	33.5 %
pH	8 to 8.5
Total Solids	5166 mg L^{-1}
Total Volatile solids	3387 mg L^{-1}
Fat	1057 mg L^{-1}
Alkalinity	1791 mg L^{-1}
COD	5945 mg L^{-1}

Table 5. Controller parameters

Symbol	Value	Unit	Symbol	Value	Unit
R_{C1}	0.6		R_{C2}	0.4	
$P_{C1,11}$	2.8×10^{-4}		$P_{C2,11}$	729	
$P_{C1,12}$	2.5×10^{-5}		$P_{C2,12}$	437	
$P_{C1,13}$	2.3×10^{-5}		$P_{C2,13}$	291	
$P_{C1,21}$	2.5×10^{-5}		$P_{C2,21}$	437	
$P_{C1,22}$	5×10^{-6}		$P_{C2,22}$	729	
$P_{C1,23}$	4×10^{-6}		$P_{C2,23}$	629	
$P_{C1,31}$	2.3×10^{-5}		$P_{C2,31}$	291	
$P_{C1,32}$	4×10^{-6}		$P_{C2,32}$	629	
$P_{C1,33}$	5×10^{-6}		$P_{C2,33}$	729	
g_{S1}	1600		g_{S2}	500	

Table 6. PSO parameters

PSO parameter	MSE $X_{2,k}$
c_1	1
c_2	2
Initial v_{id}	0
Initial p_{id}	Random
particles	8
Generations	5
Initial local MSE (mol L^{-1})	1×10^{-3}
Initial global MSE (mol L^{-1})	1×10^{-3}

Table 7. MSE Comparative

Test	MSE $X_{2,k}$	MSE Y_{CH_4}
Test 1	3.3712×10^{-6}	5.6277×10^{-5}
Test 2	1.0495×10^{-7}	1.9202×10^{-6}

Table 8. MSE Comparative

Test	MSE $X_{2,k}$	MSE Y_{CH_4}
Test 3	5.8601×10^{-7}	8.5370×10^{-6}
Test 4	1.6686×10^{-7}	2.9727×10^{-6}

B. PUBLICATIONS

B.1 Journals

K. J. Gurubel, E. N. Sánchez, F. Ornelas-Tellez and S. Carlos-Hernández, Hybrid Intelligent Inverse Optimal Control fnd or Methane Production in an Anaerobic Process, CABEQ 2012, Accepted.

K. J. Gurubel, A. Y. Alanis, E. N. Sanchez and S. Carlos Hernandez, A Neural observer with time-varying learning rate: analysis and applications, IJNS 2013, submitted.

K. J. Gurubel, E. N. Sánchez, S. Carlos-Hernández and F. Ornelas-Tellez, Integrated Hybrid Intelligent Control Scheme for Methane Production in an Anaerobic Process, IJASC 2013, submitted.

B.2 Book chapter

S. Carlos-Hernández, K. J. Gurubel and R. Carrasco, Modeling and simulation of alternative energy generation processes by using HONN, International, IGI GLOBAL, November 2012.

B.3 International conference papers

K. J. Gurubel, E. N. Sánchez, S. Carlos-Hernández and F. Ornelas-Tellez, PSO Hybrid Intelligent Inverse Optimal Control for an Anaerobic Process, CEC 2013, Cancún, QRoo, México

K. J. Gurubel, E. N. Sánchez, S. Carlos-Hernández Neuro-Fuzzy Control Strategy for Methane Production in an Anaerobic Process, IJCNN 2013, Dallas, Texas, USA.

K. J. Gurubel, E. N. Sánchez, S. Carlos-Hernández and F. Ornelas-Tellez, Speed-Gradient Inverse Optimal Neural Control for Anaerobic Digestion Processes, WAC 2012, Puerto Vallarta, Jalisco, Mexico.

K. J. Gurubel, E. N. Sanchez, and S. Carlos-Hernandez, Dynamic Learning Rate (η_D) for Recurrent High Order Neural Observer (RHONO): Anaerobic Process Application, IJCNN 2011, San jose, California, USA.

B.4 National conference papers

K. J. Gurubel, E. N. Sánchez, F. Ornelas-Tellez y S. Carlos-Hernández, Control Híbrido Inteligente Neuronal Óptimo Inverso con Gradiente de Velocidad para Producción de Metano en un Proceso Anaeróbico, AMCA 2012, Cd. Del Carmen, Campeche.

K. J. Gurubel, E. N. Sánchez, S. Carlos-Hernández y F. Ornelas, Control Neuronal Óptimo inverso para Regular la Producción de Metano en un Proceso de Digestión Anaeróbica, AMCA 2011, Saltillo, Coahuila.

K. J. Gurubel, S. Carlos-Hernández, E. N. Sánchez, Razón de Aprendizaje Dinámica para Un Observador Neuronal Recurrente de Alto Orden (RHONO): Aplicación a Un Proceso Anaeróbico", SINAFIQ 2011, Saltillo, Coahuila.
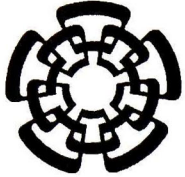
CENTRO DE INVESTIGACIÓN Y DE ESTUDIOS AVANZADOS DEL I.P.N.
UNIDAD GUADALAJARA

El Jurado designado por la   Unidad Guadalajara   del Centro de Investigación y de Estudios Avanzados del Instituto Politécnico Nacional aprobó la tesis

Control Óptimo Inverso Híbrido Inteligente para un Proceso de Digestión Anaeróbica / Hybrid Intelligent Inverse Optimal Control for an Anaerobic Digestion Process

del (la) C.

Kelly Joel GURUBEL TUN

el día 14 de Junio de 2013.

Dr. Edgar Nelson Sánchez Camperos
Investigador CINVESTAV 3D
CINVESTAV Unidad Guadalajara

Dr. Alexander Georgievich Loukianov
Investigador CINVESTAV 3C
CINVESTAV Unidad Guadalajara

Dr. José Javier Ruíz León
Investigador CINVESTAV 3B
CINVESTAV Unidad Guadalajara

Dr. Antonio Ramírez Treviño
Investigador CINVESTAV 3A
CINVESTAV Unidad Guadalajara

Dr. Salvador Carlos Hernández
Investigador CINVESTAV 2A
CINVESTAV Unidad Saltillo

Dr. Marco Antonio Perez Císneros
Profesor Titular
Universidad de Guadalajara

Dra. Alma Yolanda Alanis García
Investigador
Universidad de Guadalajara